International Journal of Modern Physics E
Vol. 26, No. 9 (2017) 1730004 (36 pages)

DOI: 10.1142/S0218301317300041

World Scientific
www.worldscientific.com

Nuclear final-state interactions in deep inelastic scattering off the lightest nuclei

W. Cosyn
Department of Physics and Astronomy,
Ghent University, Proeftuinstraat 86,
B9000 Gent, Belgium
wim.cosyn@ugent.be

M. Sargsian
Department of Physics, Florida International University,
Miami, FL 33199, USA
sargsian@fiu.edu

Received 30 June 2017
Accepted 5 July 2017
Published 3 August 2017

We review recent progress in studies of nuclear final-state interactions in deep inelastic scattering (DIS) off the lightest nuclei tagged by a recoil nucleon. These processes hold a lot of potential for resolving the outstanding issues related to the dynamics of hadronization in QCD. Within the minimal Fock component framework, valid at large Bjorken x, the main features of the theoretical approach based on the virtual nucleon approximation are elaborated. In this approach, the strong final-state interaction of the DIS products with the nuclear fragments is described by an effective eikonal amplitude, whose parameters can be extracted from the analysis of semi-inclusive DIS off the deuteron target. The extraction of the Q^2 and W mass dependences of these parameters gives a new observable in studying the QCD structure of DIS final states. Another important feature of tagged DIS off the lightest nuclei is the possibility of performing pole extrapolation with a high degree of accuracy. Such extrapolation allows an extraction of the neutron structure function in a model independent way due to suppression of the final-state interaction in the on-shell limit of the struck nucleon propagator. We review the first application of the pole extrapolation to recent experimental data. Finally, we outline the extension of the framework to inclusive DIS, including a polarized deuteron target as well as its application to the tagged DIS reactions for future experiments at fixed target and collider energies.

Keywords: Nuclear deep inelastic scattering; final-state interactions; deuteron.

PACS Number(s): 11.80.−m, 13.60.−r, 13.85.Ni

1. Introduction

QCD space-time evolution and final-state interactions: The space-time evolution of the product of deep inelastic scattering (DIS) from a nucleon or nuclear

target represents one of the important topics in modern QCD studies. As it was formulated by B.J. Bjorken "*The central question is why, when quarks are struck by leptons or other currents and one would expect to see them in the final states, one does not and only ordinary hadrons come out*".[1] Ultimately, the understanding of this process is related to the understanding of the largely unknown dynamics of QCD confinement. The quark confinement in the scattering processes, in which the energetic probe strikes an isolated quark, involves the space-time evolution of the struck quark and accompanying spectator quark–gluon system to the final hadronic state. This evolution is poorly understood despite the existence of many experiments dedicated to hadronization studies.

One way to explore the space-time evolution of the struck quark to the final hadronic state is to probe the evolving quark–gluon system's reinteraction within the medium through which it propagates. In this respect, QCD processes involving nuclear targets play a special role since spectator nucleons, not participating in the initial hard QCD scattering, can be used to monitor the space-time evolution of the produced quark–gluon system by means of final-state interactions (FSIs). With this, we introduce the *concept* of studies of the FSI of the states produced in DIS from a bound nucleon with spectator nucleons in the nuclear medium.

Need for semi-inclusiveness in nuclear DIS processes: Historically, DIS was first studied experimentally in inclusive processes, in which only the scattered probe was detected in the final state of the reaction. The integration over the wide range of produced hadronic masses in such processes makes the condition of completeness of hadronic final states almost ideal. As a result, the unitarity condition for the hadronic final states almost completely eliminates the information on their space-time evolution. Thus, the inclusive DIS process is sensitive to the initial quark–gluon state of the system (encoded in partonic distributions) and their initial state evolutions.

Studies of the space-time evolution in the final state of the reaction require some degree of exclusiveness in the reaction. This is achieved by detecting the scattered probe in coincidence with a certain hadronic component which is present in the final state of the reaction. In detecting such a hadronic component, one considers two distinct possibilities. In the *first* case, the hadronic component is the direct product of the deep inelastic scattering with the probe, while in the *second* case, the detected hadronic component emerges from the debris of the residual nucleon or nucleus.

In collider kinematics, these two scenarios of hadronic production are generally referred to as current or target fragmentation processes. They are separated by the sign of the rapidity variable η defined as

$$\eta = \frac{1}{2}\log\frac{E+p_z}{E-p_z}, \tag{1}$$

where p_z is the momentum of the detected particle (or jets) in the direction of the probe colliding with the target and E is its energy. With rapidity defined as in

Eq. (1), positive η will correspond to a hadron originating from the probe–quark interaction (current fragmentation), while the recoiling particles in the DIS process will emerge with negative η corresponding to the target fragmentation region.

In the target rest frame, these two regimes in semi-inclusive DIS are distinguished by their characteristic momenta: hadrons produced from the struck quarks carry momenta comparable with the momentum transfer in the reaction $\gg 1\,\mathrm{GeV}/c$, while the hadrons from the nuclear residual state have momenta on the order of $\sim 1\,\mathrm{GeV}/c$.

The possibility of detecting nucleons in the target fragmentation region significantly enhances the sensitivity of the reaction to the FSI of DIS products with the residual nuclear system. The main point here is that due to the factorization of the hard QCD scattering from the soft nuclear processes, the nuclear response to the DIS with production of a recoil nucleon is described by the decay function.[2,3] The decay function represents the joint probability of finding an initial "target" nucleon with given momentum and virtuality in the ground state of the nucleus and a recoil nucleon with fixed momentum in the decay products of the residual nucleus. This function can be reliably calculated within plane-wave impulse approximation (PWIA), especially for light nuclei.[4,5] Any modification of the PWIA decay function in the experimental measurement will be an indication for the final-state interaction between DIS products and residual nuclear system.

QCD dynamics and nuclear FSI: The above-discussed FSI between DIS products and the residual nuclear system represents a sensitive tool in probing the QCD mechanism of deep inelastic scattering.

To illustrate this sensitivity, we consider two distinct scenarios of DIS and indicate how their FSI dynamics can be significantly different. In Fig. 1(a), one considers the minimal Fock component mechanism of DIS (see e.g., Refs. 6 and 7). In this mechanism, the interacting virtual photon flips one of the valence quarks with the two remaining valence quarks being transferred to the final state with subsequent hard interactions between these quarks. Consequently, all valence quarks end up in the current fragmentation region. One expects such a mechanism to dominate at kinematics with large Bjorken x_{Bj} and relatively large Q^2, providing a natural transition from inelastic resonance production to the DIS regime.[8] From the point

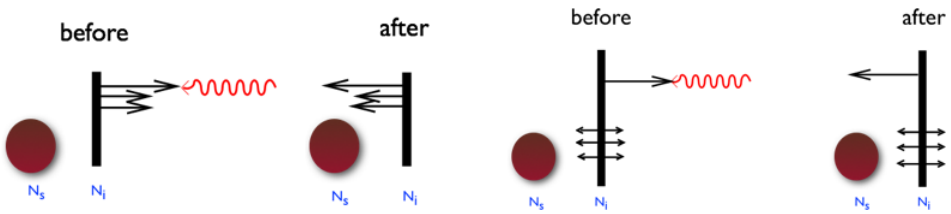

Fig. 1. (a) Minimal Fock component and (b) Feynman mechanism scenarios of DIS followed by the final-state interaction off the spectator nucleon N_s.

of view of the FSI between the products of such a deep inelastic scattering (depicted by the three left pointing arrows in the right panel of Fig. 1(a) and the spectator nucleon N_s, one observes that it will resemble the soft interaction of a fast "baryon" with the slow spectator nucleon. Thus, in such a scenario, the FSI dynamics will resemble scattering in the eikonal regime in which fast "baryon"-N_s interaction is described effectively through a diffractive-like amplitude.

In the second scenario, depicted in Fig. 1(b), we consider the Feynman mechanism[9] of DIS. In this case, the incoming virtual photon interacts with one of the quarks in the nucleon with the other quarks essentially acting as spectators and appearing in the target fragmentation region together with the spectator nucleon. In this scenario, the DIS products after the $\gamma^* N_i$-interaction are qualitatively different from that of the minimal Fock component approximation discussed in the previous paragraph. The FSI in this case is dominated by the interaction of the "wounded nucleon" (from which one quark is removed) with the spectator nucleon (N_s) in the nucleus. As the relative momentum between these two scatterers is small compared to the transferred photon momentum, this interaction is not eikonal. Consequently, it does not possess the characteristics of high-energy small-angle diffractive scattering. Such a scenario is realized in kinematics corresponding to the lower end of the valence quark region with Bjorken $x \lesssim 0.1$ and large Q^2. In this case, the produced mass for the DIS product associated with the fast quark is significantly larger than in the minimal Fock component mechanism. The struck quark most likely escapes nucleus without reinteraction, hadronizing outside the light nucleus. Such kinematics are the ones being currently discussed for the possible electron-nucleus collider (EIC) with significant capabilities for studying semi-inclusive DIS processes with tagged nucleons.[10]

In summary, the investigation of the mechanism of the FSI can provide a new approach in identifying the dynamics of the underlying deep inelastic scattering. If the specific character of the FSI is identified, then measuring its dependence on Q^2 and invariant mass W of the DIS products, as well as the dependence on the kinematic parameters of the tagged nucleon will allow one to resolve the spatial distribution of the DIS product and its space-time evolution as it propagates through the nuclear medium (see further discussion below).

Existing studies: Historically, the issues of FSIs in the nuclear medium in deep inelastic processes emerged with the advent of high-energy deep inelastic electron–nucleus, hadron–nucleus and heavy-ion scatterings. Observations such as the suppression of hadron production from nuclei in $e + A$ scattering,[11–15] suppression of high p_t production of hadrons in $h + A$ scatterings (see e.g., Ref. 16) as well as jet-quenching in heavy ion collisions (e.g., Refs. 17 and 18) indicated robust FSI phenomena in DIS in the nuclear medium.

There is a multitude of theoretical studies aimed at the understanding the observed suppressions and dynamics of propagation of DIS products in the nuclear medium (see e.g., Refs. 19–22). One of the main observations made in these studies

is that the production and propagation of hadrons in the nuclear medium in DIS at $x_B \geq 0.1$ (i.e., dominated by the valence quarks) is associated predominantly with *three dynamical phenomena*: (i) vacuum energy loss related to confinement, (ii) induced energy loss due to gluon radiation, and (iii) the processes driving the hadronization of the initial color-neutral DIS product to the final hadronic state.

The complete picture of hadron production from nuclei in DIS is described by the sequence of these three phenomena in which each process is characterized by its own time scale. These time scales are (i) the formation time, t_f — the time it takes for struck-quarks to form a color-neutral state, (ii) the coherence time, t_c — the time during which no gluon is radiated by the leading quark, and (iii) production time, t_p — characterizing the formation of the final hadron from the intermediate color-neutral state.

The dynamical content of these three processes are qualitatively different and current models predict different scale and distance dependences for the energy loss of the produced leading quark. On the qualitative level, however, these three processes take place in a strict sequence in which formation and radiation energy loss precede the production process of the final hadron.

The main focus in experimental studies of hadronization processes so far has been semi-inclusive production of leading mesons or jets from medium to heavy nuclei. For example in electroproduction processes, the main experimental observable is:

$$R_A(z_h, p_T, Q^2, \nu) = \frac{d\sigma(\gamma^* A \to hX)/dz_h d^2p_T}{A d\sigma(\gamma^* p \to hX)/dz_h d^2p_T}, \tag{2}$$

where $z_h = \frac{E_h}{\nu}$, with E_h being the energy of detected hadron and p_T, Q^2 and ν are transverse momentum of the detected hadron, virtuality and energy of the incoming photon.

The considered reaction is cumulative in nature, meaning that its cross-section is sensitive to the sum of all three above-mentioned dynamical effects. Even though within specific models one can estimate and vary the three different time scales (t_f, t_c and t_p) by specific choices of kinematic variables, one however can not vary internucleon distances in nuclei since no nuclear response is measured in these reactions. Moreover, in many theoretical models the description of the nuclear structure is rather simplistic with the nuclear medium being described as uniform with no surface effects in the estimate of nuclear transparency(the effects discussed in Ref. 23) or dynamical correlations between sequential FSIs off bound nucleons (as discussed in Refs. 24 and 25).

Paradigm shift towards the lightest nuclei: In this and the following sections, we will present arguments and demonstrate quantitatively that exploiting the lightest nuclei in deep inelastic processes can provide a new framework for studies of FSI dynamics of QCD processes. We consider semi-inclusive deep-inelastic processes

$$\gamma^* + A \to N_s + X, \tag{3}$$

in which at least one nucleon (N_s) is detected in the target fragmentation region. Reaction (3) is often referred to as *tagged* nuclear DIS. The considered light nuclear targets are the deuteron or ^{3}He (^{3}H) nuclei, whose nuclear structure can be calculated with sufficient degree of accuracy. This reaction can be further enhanced by detecting an additional hadron (h) in the current fragmentation region. Our current discussion, however, will focus mainly on the reaction (3) to demonstrate its feasibility for studies of DIS FSI.

The main argument for studies of QCD rescattering processes using the above reaction is that by identifying N_s as a spectator nucleon and measuring it at different momenta and production angles, one is able to control the effective distances between the active nucleon (on which the $\gamma^* N$ scattering took place) and the spectator nucleon on which the DIS products rescatter. The ability of tuning such distances is essential since it allows to scan the strength of DIS products rescattering off the spectator nucleon at (above discussed) different stages of fast quark hadronization. Such an approach in principle will allow to separately probe the t_f, t_c and t_p time scales of QCD hadronization.

The methodology of separation may consist of mapping out the Q^2 and W (or x) dependences of the FSI strength by comparing the actual cross-section of reaction (3) with the PWIA calculation. Another approach (discussed in the review) is to model the FSI and to extract the parameters of final-state interaction of DIS products with the spectator nucleon by fitting it to the experimental cross-sections (see e.g., Ref. 26). If one extracts the detailed Q^2 and W distributions of the FSI strength, then the analysis can proceed by identifying the analytic form of the Q^2 dependence at different momenta of the spectator nucleon. For example, if at a given momentum range of spectator nucleon one observes $1/Q^2$ dependence of the total cross-section of DIS FSI, one will be able to associate it with the time scale of propagation of the color-dipole object relevant to t_c (see e.g., Refs. 27 and 19). Softer than $1/Q^2$ with eventual disappearance of the Q^2 dependence will indicate the dominance of the t_p stage of hadronization. Finally, the evolution of the FSI strength from large x (~ 0.8) to small x (~ 0.1) region will allow to study the transition from the "eikonal" to the "wounded" nucleon regimes of the FSI discussed earlier. These examples indicate that one can consider the theoretical approaches currently employed in "traditional" hadronization studies to model Q^2 and possibly W dependences of FSI to be tested in tagged DIS reactions involving the lightest nuclei.

For the successful identification of above discussed QCD dynamics in the FSI, one needs highly accurate estimates of "conventional" nuclear effects. This emphasizes another important advantage of using the lightest nuclei, namely the possibility of calculating nuclear structure with high precision. The latter provides an important baseline for detecting and constraining FSI effects. For example, the possibility of calculating with a high degree of accuracy the nuclear decay function with a given recoil nucleon momentum in the PWIA will provide an important

baseline for detecting minute effects related to the production, rescattering and hadronization of DIS products in reaction (3).

The discussion so far was focused on reaction (3) at large momenta of the spectator nucleon, which allows to probe different stages of hadronization of the produced fast quark. It is worth mentioning that the opposite limit, corresponding to a vanishing spectator momentum, opens up a different venue for QCD studies, which is the extraction of the DIS structure function of a barely bound nucleon. In the case of tagging protons from the deuteron target, this possibility is especially valuable for the extraction of the neutron DIS structure functions, needed for flavor decomposition of parton distribution functions (PDFs).[28–30] The same reaction, now with tagged neutrons measured over the wider range of momenta in backward directions (to minimize FSI), can be used for studies of medium modification of the PDFs.[31] In this case, the possibility of varying the virtuality of interacting proton through the momentum of spectator neutron gives a unique opportunity for verifying different models introduced to describe nuclear EMC phenomena.[32]

In the following sections, we review our recent and ongoing studies of reaction (3) for the simplest case of the deuteron target. During the last several decades, progress in the determination of NN interaction potentials[33,34] as well as completion of the first high-energy deuteron electro-disintegration experiments,[35–37] allowed to confine the uncertainty of the deuteron wave function to $\sim 5\%$ for internal momenta of up to 400 MeV/c. Such a knowledge of the deuteron in the range of 0–400 MeV/c translates into internucleon distances of $\sim 4 - 1.2$ fm. This indicates that with the deuteron target, we have a femtometer scale "detector" which can provide reliable interaction measurements on inter-nucleon distances from ~ 4 fm down to 1.2 fm. This is a sufficiently wide distance scale for investigation of the above discussed QCD final-state processes with high degree of precision.

Outline: In Sec. 2, we review the theoretical framework of the virtual nucleon approximation (VNA) for calculation of DIS on the bound nucleon in the deuteron. The main goal of the approximation is the treatment of the off-shellness of the bound nucleon that becomes an important factor at large internal momenta in the deuteron. In the second part of the section, we outline the framework of the generalized eikonal approximation (GEA) which is used for the calculation of FSI in DIS processes at large Bjorken x. Section 3 presents the application of the VNA for calculation of the cross-section of the reaction (3) for the deuteron target and comparison with the first experimental data taken at Jefferson Lab. In this section, we demonstrate the sensitivity of reaction (3) to the FSI dynamics of DIS processes as well as extract the Q^2 and W dependences of the FSI parameters. While in Sec. 3, we are interested in the relatively large magnitudes of the tagged nucleon momenta (up to 400 MeV/c) aimed at the exploration of the FSI dynamics of DIS, in Sec. 4 we consider the opposite, small momentum limit of the tagged protons to extract the DIS structure function of the "free" neutron. We introduce the pole extrapolation

procedure and apply it to the recently measured data for the tagged DIS reaction off the deuteron. In Sec. 5, we extend the VNA to inclusive DIS scattering off the deuteron including FSI. Our main motivation here is to understand the role of FSI at intermediate Q^2 and large x where it can interfere with different phenomena, most importantly medium modification effects that are currently being intensively studied. Section 6 discusses the extension of VNA studies for the DIS reaction involving a tensor polarized deuteron target. Finally, in Sec. 7 we discuss further venues of studying FSI dynamics involving the lightest nuclei in collider kinematics, and consider different extensions to the semi-inclusive processes.

2. Virtual Nucleon Model for Final-State Interactions

In the following, we focus on a particular case of the reaction (3) — semi-inclusive DIS off the deuteron

$$e(l) + d(p_D) \to e'(l') + N(p_s) + X(p_X) \tag{4}$$

with the detection of a recoil nucleon N in coincidence with the scattered electron. Here l, p_D, l', p_s and p_X identify the four momenta of initial electron, target deuteron, scattered electron, recoil nucleon and the deep-inelastic final state. This reaction is commonly referred as a tagged spectator process and satisfies the semi-inclusiveness outlined in Sec. 1. The advantage of choosing a deuteron target is in the relative simplicity of describing nuclear effects and dominance of the pn component in the nuclear wave function for internal momenta of up to $700\,\mathrm{MeV}/c$. Such a dominance is associated with the higher threshold of inelastic transitions due to zero isospin of the deuteron forbidding $N\Delta$ components. Consequently the lowest mass nonnucleonic components correspond to $\Delta\Delta$ or NN^* states.

The deuteron is a very dilute system, thus no significant final-state interaction happens for processes sensitive to the average configuration of the deuteron. The possibility of measuring of the recoil nucleon at large momenta at specific kinematics, however, allows to "compress" the initial proton–neutron state to small separations significantly enhancing the FSI effects. The price one pays in considering large momentum recoil nucleons is that the external probe now scatters from a nucleon in the deuteron which is far off-shell. As a result one needs an adequate theoretical framework for the description of deep inelastic scattering from the virtual nucleon in the target.

2.1. *Virtual nucleon approximation*

There are several theoretical approaches in describing inclusive DIS from a deeply bound nucleon in the nucleus,[2,38–41] ranging from models in which the deuteron is treated nonrelativistically with off-shell effects included in the leading twist approximation, to models in which the scattering process is described in the light-front reference frame which allows to suppress the negative energy contributions in the bound nucleon propagator (referred to as Z-graphs). Some of these approaches

have been extended to semi-inclusive deep inelastic processes[31,42–46] with additional approaches for describing final-state interactions of DIS products with recoil nucleons.

An approach that allows to self-consistently describe both the reaction mechanism and final-state interactions in semi-inclusive or exclusive processes is the virtual nucleon approximation (VNA).[47,48] The VNA allows to conveniently calculate nuclear scattering amplitudes based on effective Feynman diagram rules and has been successfully applied to quasi-elastic nuclear breakup reactions[48–51] as well as photo- and electroproduction of vector mesons[52–54] and baryonic resonances[55] off nuclear targets.

In what follows, we discuss the generalization of VNA for (deep) inelastic processes focusing on the semi-inclusive reaction (4). Even though the calculations presented in the article consider a deuteron target, the obtained results can be straightforwardly applied to other nuclei.

The construction of the VNA model of nuclear DIS scattering assumes the following kinematical restrictions that justify the approximations made in the derivations: (i) Considering inelastic scattering, we require that $Q^2 > 1-2\,\mathrm{GeV}^2$ in which case the momentum of the produced state significantly exceeds the momentum of the spectator nucleon. Such a condition justifies the factorization of the scattering dynamics into a nuclear part, that describes the structure of the nuclear target, and a part containing the interaction of the probe with a bound nucleon; (ii) For DIS processes we are interested in large Bjorken x in which case the valence quarks are the main constituents of the bound nucleon in the nucleus; (iii) The momentum of the recoil nucleon is $< 700\,\mathrm{MeV}/c$, which allows us to consider only the pn component of the deuteron wave function as well as neglect the negative energy projections of the bound nucleon propagator.

The above assumptions allow to describe the reaction (4) through the sum of two Feynman diagrams, depicted in Fig. 2, which correspond to the impulse approximation (IA) and FSI contributions to the scattering process. The calculations then proceed by applying effective Feynman diagrammatic rules to these diagrams.[26]

Since Feynman diagrams are manifestly covariant the relativistic kinematics enter in the calculation self-consistently both in the interaction of the virtual photon with the bound nucleon as well as in the final-state interaction of DIS products off the spectator nucleon.

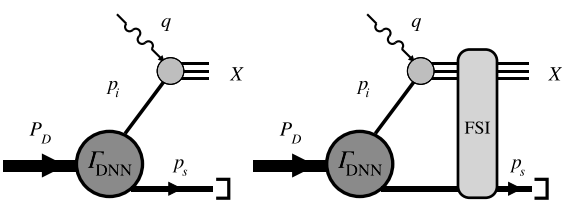

Fig. 2. VNA Feynman diagrams for the impulse approximation (left) and final-state interaction (right) contributions to the tagged nucleon DIS reaction from a deuteron target.

The two main approximations of VNA are: (i) treating spectator nucleons as on-mass shell and (ii) accounting only for the positive energy projection of the bound nucleon propagator (thus neglecting Z-graphs in which an anti-nucleon propagates backwards in time). These two approximations are implemented technically by estimating the loop integrals in the scattering amplitude through the positive energy pole of the spectator nucleons and reconstructing the kinematic parameters of $\gamma^* N_{\rm bound}$ scattering through energy-momentum conservation at the nucleus $\to$ nucleons transition (DNN) vertex. The latter will result in a virtual bound nucleon with four-momentum square less then the rest mass square.

The above procedure in VNA allows to relate the DNN transition vertex appearing in Fig. 2 to the deuteron wave function,[26,51,56] which is defined as follows:

$$\Psi^{\lambda_D}(\boldsymbol{p}_i,\sigma_i;\boldsymbol{p}_s,\sigma_s) = -\frac{\bar{u}(p_i,\sigma_i)\Gamma^{\mu}_{DNN}\epsilon(\lambda)_{\mu}u_{\mathcal{C}}(\boldsymbol{p}_s,\sigma_s)}{\sqrt{4E_s(2\pi)^3}(p_i^2-m_N^2)}, \tag{5}$$

where $u_{\mathcal{C}}(\boldsymbol{p}_s,\sigma_s) = -i\gamma_2 u^*(\boldsymbol{p}_s,\sigma_s)$ is the charge conjugated spinor and $\epsilon(\lambda)_{\mu}$ is the polarization four-vector of the deuteron. The above defined wave function corresponds to the solution of the relativistic Bethe–Salpeter type equation in the spectator nucleon approximation (see e.g., Ref. 57). Such a wave function satisfies the baryon number conservation sum rule[58]:

$$\sum_{\lambda_D\sigma_i\sigma_s}\int d^3\boldsymbol{p}_i\alpha_i|\Psi^{\lambda_D}(\boldsymbol{p}_i,\sigma_i;\boldsymbol{p}_s,\sigma_s)|^2 = 1, \tag{6}$$

where $\alpha_i = 2-\alpha_s$ is the light-front momentum fraction of the deuteron carried by the struck nucleon

$$\alpha_i = \frac{2p_i^-}{p_D^-} = 2-\frac{2(E_s-p_{s,z})}{M_D}. \tag{7}$$

This sum rule can be obtained by considering the conservation of baryon number in the VNA or the normalization of the nuclear charge form-factor at zero momentum transfer ($F_A(0) = Z$).[48] However, the wave function does not saturate the momentum sum rule:

$$\int \alpha_i^2 \sum_{\lambda_D\sigma_i\sigma_s}|\Psi^{\lambda_D}(\boldsymbol{p}_i,\sigma_i;\boldsymbol{p}_s,\sigma_s)|^2 d^3\boldsymbol{p}_i < 1 \tag{8}$$

which can be attributed to the contribution of nonnucleonic components neglected in VNA approximation.

As the virtual photon interacts with an off-shell bound nucleon, a prescription for the off-shell part of the bound nucleon propagator is needed. In the VNA, this off-shell part of the propagator is dropped in the nucleonic current[26] and gauge invariance is restored by expressing the component of the hadronic current along the three-momentum transfer through the time-component of the hadronic current, using

$$q_\mu J^{\mu}_{\gamma^* N_{\rm bound}} = 0. \tag{9}$$

However, even with gauge invariance restored, the inelastic currents are largely unknown for numerical estimates. To proceed one introduces the hadronic tensor of the inelastic $\gamma N_{\rm bound}$ scattering, $W_N^{\mu\nu} \sim J^{\mu,\dagger}_{\gamma^* N_{\rm bound}} J^{\nu}_{\gamma^* N_{\rm bound}}$ which enters in the square of the IA part (Fig. 2(a)) of the nuclear scattering amplitude. The latter is expressed through the inelastic nucleon structure functions $F_{1N}(\tilde{x}, Q^2)$ and $F_{2N}(\tilde{x}, Q^2)$ which are evaluated using phenomenological parametrizations available from experimental DIS measurements. Note that $\tilde{x}$ in the argument of the structure functions represents the Bjorken scaling variable in which the bound nucleon virtuality is taken into account (see Eq. (16)).

To perform a similar procedure for the FSI case (Fig. 2(b)) one needs an additional approximation that allows to factorize the inelastic electromagnetic current (9) from the loop integral which is present in the FSI amplitude. This factorization assumption (commonly referred to as the distorted-wave impulse approximation or DWIA) is valid for $\sqrt{Q^2} \gg p_s$, in which case the nucleon current becomes insensitive to the initial momentum of the struck nucleon. The factorization assumption has been verified in quasi-elastic deuteron breakup calculations, where a comparison with unfactorized calculation is possible. It was found that for $Q^2 \sim 4\,{\rm GeV}^2$ the factorization holds for recoil nucleon momenta of up to $400\,{\rm MeV}/c$. At larger momenta DWIA calculations systematically underestimate the unfactorized calculations.[51]

2.2. *Generalized eikonal approximation*

To calculate the FSI, we take into account the kinematic restriction (ii) of the previous section, namely we consider large Bjorken x which justifies the minimal-Fock component approximation of the partonic structure of the nucleon. In this case we adopt the scenario of Fig. 1(a) for the FSI of DIS products X with the spectator nucleon in the deuteron. If the momentum of the X system significantly exceeds the momentum of the spectator nucleon, the FSI will be dominated by diffractive scatting, which allows us to use the framework of the generalized eikonal approximation (GEA).[47,48] Because the starting point of the calculation is based on the effective Feynman diagrammatic approach which is covariant, the GEA preserves the relativistic dynamics of the FSI with the spectator nucleon which has finite momentum. As such the spectator nucleon cannot be considered a stationary scatterer, as in a conventional Glauber approximation. One manifestation of the relativistic dynamics is the approximate conservation of the light-front momentum fraction of the spectator nucleon, α_s in the process of FSI.[48] This conservation results in the GEA prediction that in quasi-elastic scattering FSI peaks at $\alpha_s = 1$ rather than at spectator angles $\theta_{\rm sq} = 90^0$ (relative to the momentum transfer) as it is expected in the conventional Glauber approximation. For $p_s = 400\,{\rm MeV}/c$ the condition $\alpha_s = 1$ corresponds to $\theta_{\rm sq} \approx 70^0$ which was observed experimentally in the recent quasi-elastic deuteron electrodisintegration measurements[35–37] performed in $Q^2 > 1\,{\rm GeV}^2$ kinematics.

For deep-inelastic processes, the challenge in describing final-state interactions lies in the fact that for the produced X-state both its composition and space-time evolution are to a large extent unknown. In order to use GEA, we impose an additional constraint (consistent with the large Bjorken x kinematics) that:

$$q \gg M_X, M_{X'} \tag{10}$$

with M_X,$M_{X'}$ denoting the invariant masses of the DIS states in the final and intermediate states of the reaction. This constraint justifies the assumption of diffractive small angle rescattering for which we can consider the DIS product X as a superposition of coherent states whose interaction with the spectator nucleon can be described as:

$$\sum_{X'} f_{X'N,XN} = f_{XN}(t, Q^2, x) = \sigma_{\rm tot}(Q^2, M_X)(i + \epsilon(Q^2, M_X))e^{\frac{B(Q^2,M_X)}{2}t}, \tag{11}$$

where the sum of the all possible $X'N \to XN$ amplitudes is expressed in terms of an effective diffractive amplitude, $f_{XN}(t, Q^2, x_{Bj})$, with effective total cross-section $\sigma_{\rm tot}$, real part, ϵ and slope factor B. The latter parameters depend on the Q^2 and the invariant mass of the produced DIS state M_X. Contrary to the case of quasi-elastic processes, where these parameters can be inferred from NN-scattering data, they are not known for DIS processes and one has to calculate them based on specific models of production and hadronization of deep-inelastic states discussed in Sec. 1.

The important advantage of the considered reaction (4), however, is in the possibility of employing an opposite logic in which one obtains the (Q^2, W) dependence of the FSI parameters by fitting the experimental data. Then from these parameters the information on the QCD dynamics of the production and hadronization of deep-inelastic final states can be exctracted. An example of the latter approach is discussed in the next section.

Another difference compared to quasi-elastic processes is that due to the inelastic nature of the DIS the FSI itself can be inelastic. Thus, the invariant masses of the produced hadrons before and after the rescattering does not need to be the same ($M_{X'} \neq M_X$). One can obtain an additional constraint on these masses taking into account Eq. (10) and the above mentioned approximate conservation of light-front momentum fraction of the slow spectator, α_s in the rescattering,[48] resulting in

$$p_s^- - p_{s'}^- = p_{X'}^- - p_X^- \approx 0. \tag{12}$$

This conservation law follows from the assumption (10), which leads to $p_X^- \approx \frac{m_X^2 + p_{X\perp}^2}{2q^+} \approx 0$ (and a similar condition for $p_{X'}^-$). Using this relation and considering kinematics in which

$$p_{s\perp}^2 < k_\perp^2 \sim \frac{2}{B}, \tag{13}$$

where $k_\perp^2 = (p_s - p_{s'})^2$ is the average transferred momentum in the rescattering one obtains:

$$m_X^2 = (p_{X'} + p_{s'} - p_s)^2$$
$$\approx m_{X'}^2 - 2p_{X'\perp}(p_{s'\perp} - p_{s\perp}) - k_\perp^2 \approx m_{X'}^2 + k_\perp^2 > m_{X'}^2, \tag{14}$$

where the above derivation uses the fact that in the limit of Eq. (13) $p_{X'\perp} = -p_{s'\perp} \approx k_\perp$. The result of Eq. (14) qualitatively means that in the situation in which two "almost" collinear ($\frac{|p_{s,\perp}|}{q}, \frac{|p_{X,\perp}|}{q} \ll 1$) particles are produced by the inelastic diffractive scattering of fast and slow particles with equal and opposite transverse momenta, the mass of the final fast particle is larger than the initial mass.[26] The condition (14) maximizes the FSI in the forward direction of the spectator nucleon production (where forward refers to spectator angles $\theta_{\rm sq} \ll 90^\circ$ in the deuteron rest frame with the z-axis along the virtual photon momentum), see Sec. 3. It is worth mentioning that this feature is very different from the quasi-elastic case in which the maximum of FSI corresponds to $\alpha_s \approx 1$ (resulting in $\theta_{\rm sq} \approx 70^0$ for $p_s = 400\,\text{MeV}/c$), with the FSI diminishing in the forward direction.[51]

3. Semi-Inclusive Inelastic Scattering Off the Deuteron with Tagged Spectator

Based on the theoretical framework described in the previous section, in Sec. 3.1, we calculate the cross-section of reaction (4) in inelastic kinematics. In Sec. 3.2, we use the calculated cross-sections to analyze the first experimental data obtained in the *Deeps* experiment,[59] in which reaction (4) was measured for a wide range of spectator proton angles and momenta.

3.1. *Cross-section formulas*

For the case of unpolarized electron scattering from an unpolarized target at rest and with no polarizations being measured in the final state, the differential cross-section of reaction (4) can be presented through four independent structure functions as follows:

$$\frac{d\sigma}{dxdQ^2 d\phi_{e'} \frac{d^3p_s}{2E_s(2\pi)^3}} = \frac{2\alpha_{\rm EM}^2}{xQ^4}\left(1 - y - \frac{x^2y^2m_N^2}{Q^2}\right)\left(F_L + \left(\frac{Q^2}{2\boldsymbol{q}^2} + \tan^2\frac{\theta_e}{2}\right)\frac{\nu}{m_N}F_T\right.$$
$$\left. + \sqrt{\frac{Q^2}{|\boldsymbol{q}|^2} + \tan^2\frac{\theta_e}{2}}\cos\phi F_{TL} + \cos 2\phi F_{TT}\right). \tag{15}$$

Here, $\alpha_{\rm EM}$ is the fine-structure constant, $-Q^2 = \nu^2 - \boldsymbol{q}^2$ is the four-momentum transfer squared, Bjorken $x = \frac{Q^2}{2m_N\nu}$ (with m_N the nucleon mass), $y = \frac{\nu}{l^0}$, and ϕ is the azimuthal angle between the scattering $(\boldsymbol{l}, \boldsymbol{q})$ and spectator production $(\boldsymbol{q}, \boldsymbol{p}_s)$ planes. The four structure functions F_L, F_T, F_{TT}, F_{TL} contain all the dynamics of the virtual photon–deuteron interaction, and depend on Q^2, the Bjorken variable

defined for the interacting bound nucleon,[a]

$$\tilde{x} = \frac{Q^2}{2p_i q}, \tag{16}$$

and the tagged nucleon momentum $\boldsymbol{p}_s$. After imposing the gauge invariance condition of Eq. (9), the semi-inclusive structure functions can be expressed through the time- and transverse- components of the hadronic tensor:

$$W_D^{\mu\nu} = \frac{1}{4\pi M_D}\frac{1}{3}\sum_X \overline{\sum_{\text{spins}}} \langle D\lambda_D|J^{\dagger\mu}|X\sigma_x; p_s\sigma_s\rangle\langle X\sigma_x; p_s\sigma_s|J^{\nu}|D\lambda_D\rangle$$
$$\times (2\pi)^4\delta^4(q + p_D - p_s - p_X), \tag{17}$$

where $\overline{\sum}_{\text{spins}}$ represents the sum over the final and averaging over the initial state polarizations. The sum over X denotes a summation over the produced hadronic channels including phase space integration in each channel. Explicit expressions for the structure functions in components of the hadronic tensor can be found in Ref. 26, Sec. IIA.

Within the VNA/GEA approximation outlined in Sec. 2, we only need to consider the two diagrams of Fig. 2: (left) the IA amplitude where no reinteraction takes place between the spectator nucleon and DIS products of the $\gamma^* N$ interaction and (right) the effective FSI diagram which accounts for the reinteracton of the DIS products with the spectator nucleon. In the latter case we assume that the proton detected in the final state is the one which emerged from the deuteron as a spectator. In this case, we neglect possible contributions in which the proton originates from the DIS products produced in the spectator kinematics.

Using the effective Feynman diagram rules for the IA and FSI diagrams (for a detailed derivation see Ref. 26), and within the distorted wave impulse approximation one obtains the following expression for the hadronic tensor:

$$W_D^{\mu\nu} = W_N^{\mu\nu} S^D(p_s)(2\pi)^3 2E_s, \tag{18}$$

where the nucleon hadronic tensor $W_N^{\mu\nu}$ is normalized in analogous manner as Eq. (17) and one obtains for the distorted deuteron momentum distribution:

$$S^D(p_s) \equiv \frac{1}{3}\sum_{\lambda_D,\sigma_s,\sigma_i}\left|\Psi^{\lambda_D}(p_i\sigma_i; p_s\sigma_s) - \sum_{X'}\int \frac{d^3p_{s'}}{(2\pi)^3}\frac{\beta(s_{XN}, M_{X'})}{4|\boldsymbol{q}|\sqrt{E_s E_{s'}}}\right.$$
$$\left.\times\langle X\sigma_x; p_s\sigma_s|f_{X'N,XN}(s,t)|X'\sigma_x; p_{s'}\sigma_s\rangle\frac{\Psi^{\lambda_D}(p_{i'}\sigma_i, p_{s'}\sigma_s)}{[p_{s',z} - p_{s,z} + \Delta + i\epsilon]}\right|^2, \tag{19}$$

where

$$\beta(s_{XN}, M_{X'}) = \sqrt{(s_{XN} - (m_N - M_{X'})^2)(s - (m_N + M_{X'})^2)} \tag{20}$$

[a]Note that $\tilde{x} = 1$ does not correspond to elastic scattering as the initial nucleon is off its mass shell.

with s_{XN} being the invariant mass of the rescattering $X - N_s$ system, and

$$\Delta = \frac{\nu + M_D}{|\boldsymbol{q}|}(E_s - E_{s'}) + \theta(M_X - M_{X'})\frac{M_X^2 - M_{X'}^2}{2|\boldsymbol{q}|}, \tag{21}$$

where the Heaviside function in the second term reflects the condition of Eq. (14). If one only considers the IA diagram, the second term in Eq. (19) does not contribute, resulting in the standard convolution formula for ed scattering with the unpolarized deuteron momentum distribution. In Eq. (19), the $p_{s'}^z$ integration in the loop integral can be performed analytically, making use of the parametric form of the deuteron wave function.[26] This integration splits the rescattering contribution into on-shell and off-shell parts corresponding to on- and off- shell conditions for the intermediate X' state. For the on-shall part of the rescattering one uses the parameterization of Eq. (11) for the $X - N_S$ rescattering amplitude, while for the off-shell part an additional suppression of the amplitude of Eq. (11) is assumed to account for the extra momentum transfer needed to bring the intermediate state into the final on-shell X state. Our comparisons with the *Deeps* data in Sec. 3.2 support such an assumption.[26]

3.2. *Comparison with data*

In recent years, the reaction (4) with tagged protons has been measured in two dedicated experiments performed by the CLAS collaboration at Jefferson Lab (JLab). The first, *Deeps* ($d(ee'p_s)X$) experiment measured tagged protons in the momentum range of 300–560 MeV/c and angular range of $-0.8 \leq \cos\theta \leq 0.8$.[59] The main motivation of the experiment was to explore the signatures of medium modification of the bound neutron after identifying the kinematics where the FSI effects are negligible. The second, barely off-shell neutron scattering (BONuS) experiment focused at the lower end of the tagged proton momenta 70–150 MeV/c with the main goal of extracting the quasi-free neutron structure function.[29,60,61] In the future three similar experiments are planned at the upgraded 12 GeV JLab facility[62–64] which will cover a wider range of Q^2 and W.

Given the kinematics, the *Deeps* data provided an excellent opportunity to test and constrain the FSI model outlined in Sec. 2. Already with an educated guess for the rescattering parameters of Eq. (11), consistent with the $NN \to NN$ scattering values, the agreement achieved with the data was quite good[26] (see also Fig. 6 (right panel)). This indicated that one now can use Eq. (11) as an ansatz for exploration of the reinteraction of the DIS products with the spectator nucleon.

One particular approach is to learn about the $W \equiv M_X$ and Q^2 dependences of the FSI amplitude in Eq. (11) by constraining its parameters through fitting the *Deeps* data over the whole kinematic range of the experiment. Figures 3 and 4 show such a fit in which the effective cross-section $\sigma_{\rm tot}(Q^2, W)$, and slope parameter $\beta(Q^2, W)$ have been fitted with ϵ being fixed at the value of $\epsilon = -0.5$. The data in the figures are presented in the form of reduced cross-sections, which in the factorized DWIA correspond to the product of the neutron structure function, F_2 and

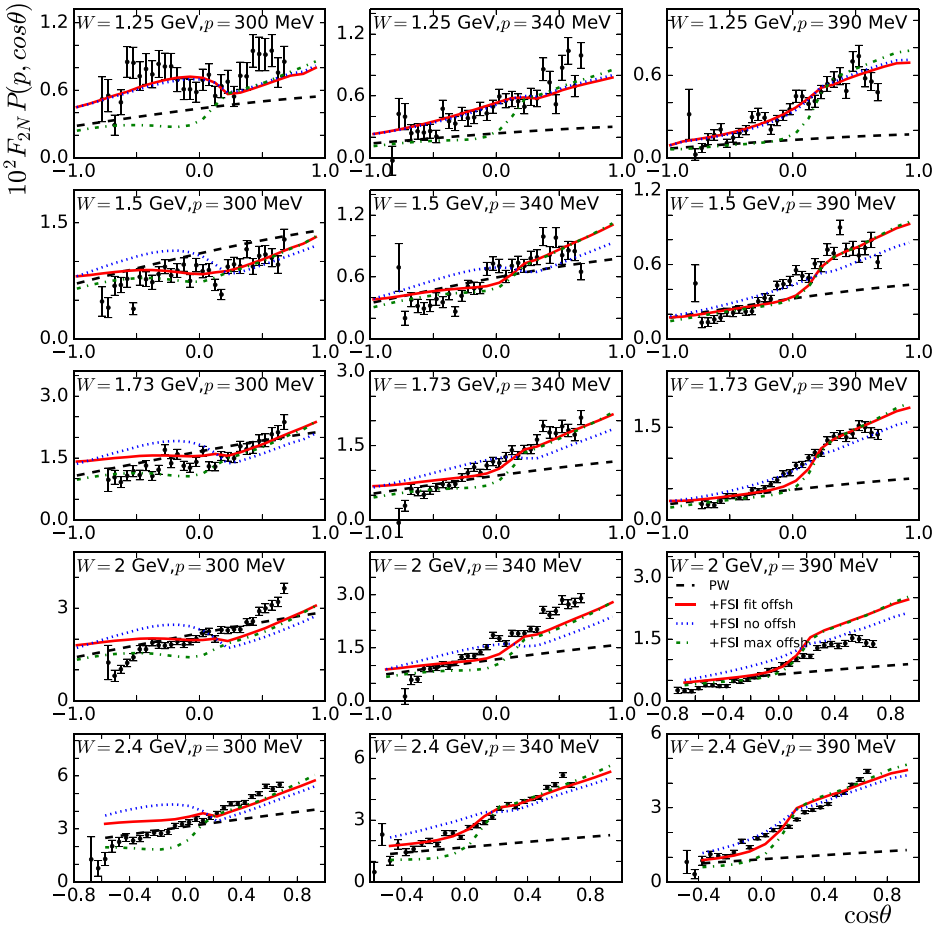

Fig. 3. (Color online) Comparison between the Deeps data[59] and VNA model calculations at $Q^2 = 2.8$ GeV^2 at measured values of invariant mass $M_X \equiv W$ and spectator proton momenta $p_s = 300, 340, 390$ MeV as a function of the cosine of the angle θ between virtual photon and tagged proton. The dashed black curves are IA calculations, the others include FSI. The effective total cross-section and slope parameter in the final-state interaction amplitude are fitted for each W, the real part is fixed at $\epsilon = -0.5$. The dot-dashed green curves consider only the on-shell rescattering, the dotted blue curves include off- and on- shell rescattering amplitudes in equal proportions and the full red curves use a suppressed off-shell parameterization.[26] Figure adapted from Ref. 26.

the distorted momentum distribution $S^D(p_s)$. The VNA/FSI calculations match the normalization of the data and reproduce the angular distribution of the data reasonably well, describing the huge rise of the reduced cross-section at forward spectator proton angles. It is worth mentioning that this rise differs qualitatively from the IA calculation which produces a fairly flat angular dependence. One also observes that the differences between different prescriptions in evaluation of the off-shell part of the rescattering[26] are quite small. Only at momenta of 300 MeV/c,

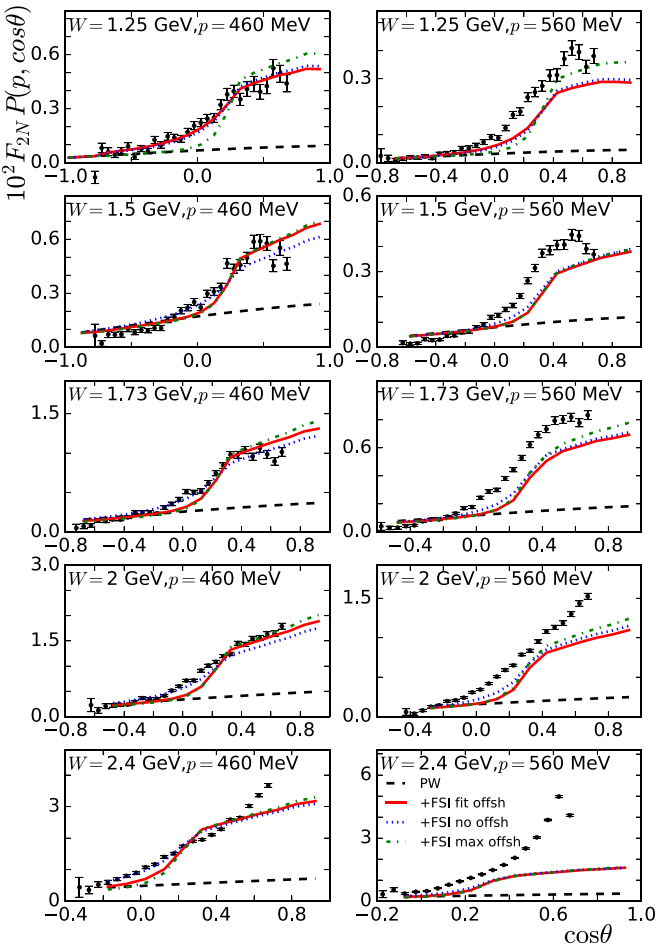

Fig. 4. As in Fig. 3 but with $p_s = 460, 560$ MeV. Figure adapted from Ref. 26.

where the contributions from IA–FSI interference and square of the FSI amplitude largely cancel each other, stronger sensitivity to the off-shell part of the rescattering amplitude is observed. In general, the data seem to favor the fits with suppressed or no off-shell contribution in the rescattering. At the highest proton momenta, the FSI calculations systematically underestimate the data. We identify two possible causes of this behavior: (i) as it was mentioned in Sec. 2, the factorization assumptions in the FSI model are increasingly inaccurate at $p_s >$ MeV/c, and (ii) at larger spectator momenta in the forward direction, the protons from the current fragmentation region are contributing to the spectator kinematics, thus enhancing the cross-section in forward directions at large values of p_s.

Once such a fit of the data is achieved one can now extract the parameters of the rescattering amplitude. Figure 5 shows the dependence of the fitted effective

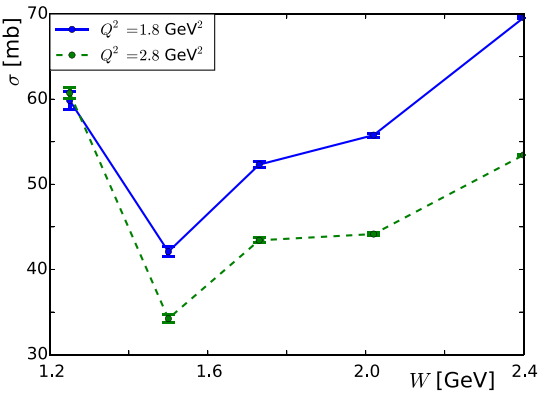

Fig. 5. (Color online) Values of the fitted $\sigma_{\rm tot}$ rescattering parameter in Eq. (11) for $Q^2 = 1.8$ GeV^2 (dashed green curve) and $Q^2 = 2.8$ GeV^2 (full blue curve), obtained by fitting the high momentum spectator deeps data. Figure adapted from Ref. 26.

cross-section parameter $\sigma_{\rm tot}$ on the invariant mass of the DIS products, W and Q^2 of the virtual photon in a fit in which the slope, β and ϵ parameters have been kept fixed (obeying constraints from unitarity). Two trends are worth highlighting. First, after an initial peak for the lowest magnitude of W corresponding to the excitation of the Δ-resonance, the effective cross-section systematically rises with invariant mass of the DIS products. This agrees with the qualitative picture, as with an increase of W more and more pions are created that can cause rescatterings. At higher W (low x), however, one expects to see a plateau for the effective cross-section, as the formation time of the hadrons grows larger and the hadronization of the struck quark will largely occur outside the nuclear medium. There is no sign of a plateau yet in the fit to the *Deeps* data.

To evaluate the Q^2 dependence of the $\sigma_{\rm tot}$, we compare two different values of Q^2 observing that the higher Q^2 bin results in smaller effective cross-sections. Such a behavior is again consistent with the qualitative picture of hadronization in QCD, in which higher Q^2 corresponds to a smaller space separation of the produced quarks. This could be interpreted as a sign of color transparency (CT)[65] in the deuteron, in which the "pre-hadron" gets produced in a smaller sized configuration at high Q^2 and experiences reduced color interactions with the medium. More data at higher Q^2 values are needed however to confirm if the observed trend indeed persists over a wide energy range. We note that other fits than those shown in Fig. 5 with more free parameters did not produce significantly better χ^2 values and showed similar trends for the $\sigma_{\rm tot}$ parameter.

The calculations presented in Figs. 3 and 4, together with the result of the extraction of the W and Q^2 dependences of $\sigma_{\rm tot}$ shown in Fig. 5 can be considered as a "proof of the principle" that such an approach can be used to investigate the hadronization process utilizing light nuclei such as the deuteron. The possibility of a detailed mapping of the W and Q^2 dependences of the FSI amplitude will allow

the analysis of the final state of the DIS from production to hadronization stage. With the 12 GeV operations underway at JLab more data will hopefully become available in the future that will allow the realization of such a program.

To conclude this section, it is worth illustrating the striking difference between the dynamics of deuteron disintegration in the quasi-elastic and DIS regime in the high Q^2 limit. In quasi-elastic electro-disintegration of the deuteron, the FSI is due to elastic $NN \to NN$ scattering which peaks at angles of $\sim 70°$–$80°$ of the spectator nucleon production, while decreasing further in both forward and backward directions (see Fig. 6 (left panel)). The suppression in the forward direction is due to the constraint of $W_N = m_N$ in the intermediate and the final state of the reaction which suppresses the phase space of the rescattering. The suppression in the backward direction is expected in the eikonal approximation due to larger momentum transfer required in the FSI amplitude to produce spectators at larger angles.[51]

For the DIS case, the picture is qualitatively different. As can be seen in Fig. 6 (right panel) — as well as in Figs. 3 and 4 — we observe that FSI results in a sizable rise of the cross-section in the forward direction of the spectator nucleons. This is caused by the condition of Eq. (14), reflected in the propagator poles of Eq. (19). The physical reason for such a rise, is that the produced mass in the intermediate state of the reaction is not constrained. As a result the final X state has larger phase space to rearrange its invariant mass and minimize the internal momenta thus maximizing the rescattering amplitude. For the backward direction of spectator nucleon production one observes the suppression of the FSI. However, such a suppression is quite nuanced. While for larger spectator momenta $p_s >$

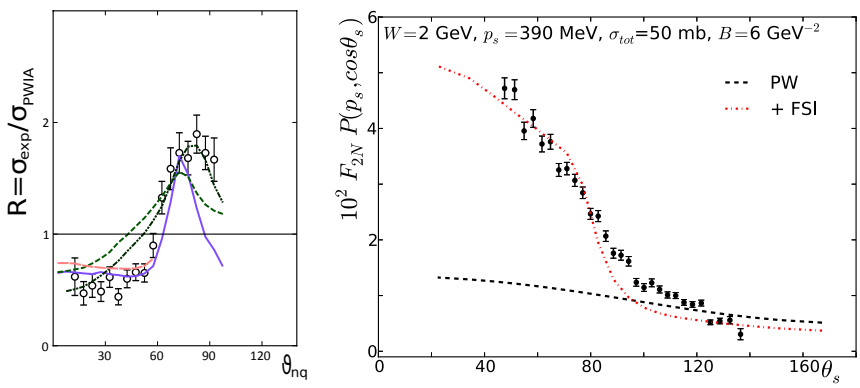

Fig. 6. (Left panel) Reduced cross-section R of quasi-elastic electro-disintegration of the deuteron as a function of spectator neutron angle θ_{nq} at neutron momentum $p_s = 400\,\mathrm{MeV}/c$. Figure adapted from Ref. 36. The different curves correspond to different FSI models discussed in Ref. 36. (Right panel) Reduced cross-section of deep-inelastic electrodisintegration of the deuteron as a function of spectator proton angle θ_s at proton momentum $p_s = 390$ MeV/c, discussed in the current text. Figure adapted from Ref. 26.

300 MeV/c (*Deeps* kinematics), the comparisons between model and data supports the small contribution of FSI effects, at lower spectator momenta (up to 150 MeV/c) this is generally not true as the BONuS data show. In the latter case there is a clear angular dependence in the backward region resulting in a noticeable difference in normalization between IA and FSI calculations (see Sec. 4.2).

4. Pole Extrapolation in Semi-Inclusive DIS Off the Deuteron

4.1. *General concept and application to the neutron structure function*

Understanding of the dynamics of the u- and d-quark interaction at large Bjorken x region of nucleon structure functions is one of the important unresolved issues in QCD. It is not clear how a single quark acquires the total momentum of the nucleon in the $x \to 1$ limit. There are a multitude of models ranging from mean-field di-quark to short-range quark–quark correlation models which predict vastly different results for the u and d quark distributions in $x \to 1$ limit.[66] One way of experimental verification of these predictions is independent measurements of the neutron and proton deep inelastic structure functions in large x limit. Due to the lack of free neutron targets, the neutron structure function measurements are performed using deuteron or ^{3}He nuclei (the latter being used mainly for the extraction of polarized structure functions).

For the case of the deuteron target, the majority of experiments considered inclusive $d(e, e')X$ scattering in which case the proton contribution was subtracted from the deuteron cross-section within a specific model that accounted for nuclear effects. These nuclear effects include relativistic motion of the bound nucleons, medium modification of nucleon structure functions, and possible contribution from nonnucleonic components. These effects, however, become increasingly important and increasingly uncertain at higher x where most of the interest in the neutron structure function lies. One of the main reasons of such uncertainty is that at large Bjorken x the inclusive reaction is strongly sensitive to the high-momentum part of the deuteron wave function which is poorly known above bound nucleon momenta in the 500 MeV/c range. This situation is reflected in the fact that currently no model of the high x distribution of u and d quarks is unambiguously ruled out, with the extracted PDFs being strongly model dependent starting at $x > 0.6$.[66]

One method that circumvents several of the issues outlined above, is performing the pole extrapolation procedure to the reaction (4) in DIS kinematics in which the spectator proton is measured at smaller momenta.[28,30,67] The pole extrapolation method was originally proposed by Chew and Low[68] for probing the structure of free π mesons or the neutron by studying $h + p \to h' + \pi + N$ reactions. In general terms, one starts from a (hadronic or electroweak) probe h and a target A consisting of two constituents, B and C. In the measurement of the reaction $h + A \to h' + X + C$ the constituent C is detected as a spectator to the underlying $h + B \to h' + X$

reaction. Figure 2(a) illustrates this for the reaction (4) in which case $A = D$ and $B = n$ and $C = p$.

Within the IA the amplitude of the process is expressed in the form:

$$M_{\rm IA} = M^{h+B\to h'+X}\frac{G(B)}{t-M_B^2}\chi_C^\dagger\Gamma^{A\to BC}\chi_A, \tag{22}$$

where χ_A and χ_C represent the wave functions of the incoming composite particle A and outgoing spectator particle C. The vertex $\Gamma^{A\to BC}$ characterizes the $A \to BC$ transition and the propagator of bound particle B is described by $\frac{G(B)}{t-M_B^2}$, with momentum transfer $t = (p_A - p_C)^2$. As it follows from Eq. (22), the IA amplitude has a singularity in the nonphysical limit $t \to M_B^2$, which corresponds to imaginary recoil momenta p_C. In Eq. (17), the singularity is present in the deuteron wave function that appears in the first term of the momentum distribution of Eq. (19).

Non-IA diagrams for process (4), such as the FSI diagram of Fig. 2(b), have an additional loop integration (see the second term of Eq. (19)) and consequently do not contain a singularity at $t \to M_B^2$. This is the content of the so-called loop theorem introduced in Ref. 28, according to which any additional (to IA) interaction contributing to the reaction $h + A \to h' + X + C$ will only have a finite contribution in the $t \to M_B^2$ limit. Consequently in such limit only the IA term contributes to the pole which now contains the $M^{h+B\to h'+X}$ amplitude on its mass shell at the singularity point of the bound "B" particle's propagator.

The deuteron is especially suited for pole extrapolation as its small binding energy ($\epsilon_B = 2.2\,\text{MeV}$) results in a very small extrapolation length into the unphysical region corresponding to small imaginary spectator momentum in the deuteron center of mass frame. In practice for the tagged DIS process of Eq. (4) the pole extrapolation is carried out by multiplying the measured quantity (e.g., the ϕ-averaged cross-section of Eq. (15)) by a factor $I(\alpha_s, \boldsymbol{p}_{s\perp}, t)$[28] which cancels the $(t-m_N^2)^2$ pole and is normalized in such a way that the structure function of interest is recovered at the on-shell point. For the F_{2n} structure function, in reaction (4), the proton is detected as a spectator and the extracted structure function is defined as

$$F_{2n}^{\rm extr}(Q^2, x, t) = I(\alpha_s, \boldsymbol{p}_{s\perp}, t)F_{2D}^{SI,\rm EXP}(Q^2, x, \alpha_s, \boldsymbol{p}_{s\perp}), \tag{23}$$

where $F_{2D}^{SI,\rm EXP}$ is the measured structure function of the deuteron for ϕ averaged cross-section of Eq. (15). As it was mentioned above the factor $I(\alpha_s, \boldsymbol{p}_{s\perp}, t)$ is normalized in such way that

$$\lim_{t\to m_N^2} F_{2n}^{\rm extr}(Q^2, x, t) = F_{2n}(Q^2, x), \tag{24}$$

with FSI effects effectively dropping out in this limit.

4.2. *Pole extrapolation of BONuS data*

Given the range of measured spectator proton momenta (70–150 MeV) in the above mentioned BONuS experiment,[29,60,61] its data provided the first real opportunity to

perform pole extrapolation procedure for the extraction of the on-shell F_{2n} structure function of the neutron using Eq. (23).[30] However before such an extrapolation is performed one needed to take into account the fact that the BONuS data suffered from a poorly known detector efficiency which varied with proton momentum. As a result their published data was normalized based on a IA model for backward proton angles. Since we have a model that accounts also for FSI effects, in Ref. 30 we used the extracted parameters of the FSI amplitude (Eq. (11)) from the fits of the *Deeps* data to calculate the cross-sections of the reaction (4) for BONuS kinematics. Then we used these calculations to obtain the overall normalization factor that now includes FSI effects. The determination of the normalization factors was done for kinematics where the uncertainties on F_{2n} are small, i.e., for the high Q^2 and low x bins of the experimental data set. These normalization factors were then applied to the whole data set, for specific details we refer to Ref. 30.

The comparison with the BONus data using the overall normalization is shown in Fig. 7. The figure compares calculations for one electron beam energy and Q^2 bin, other bins show similar results. The published data are shown as ratios of the data to an IA model used in Ref. 60. As Fig. 7 shows, the FSI calculations reproduce the angular dependence of the data reasonably well, with the highest W bins slightly underperforming. In comparison, the IA calculations again show flatter angular dependence which is in disagreement with the data. The overall conclusion is that even for such a small momenta of spectator protons the FSI effects are not negligible.

After the normalization, the pole extrapolation was performed for each $\{x, Q^2\}$ bin in the BONuS data set, where the final result was obtained as a weighted average over all spectator angle bins. The results, presented in the form of the ratios of F_{2n}/F_{2p} are shown in Fig. 8. In the $x < 0.5$ region, the extracted values are in good agreement with the existing phenomenological fit of inclusive data[69,70] and with the BONuS result.[29] In the $x > 0.5$ region, where one expects the nuclear effects to become important, a surprising rise of the ratio is observed, caused by the magnitude of F_{2n} which is larger than the one obtained from the analysis of the inclusive data. It is worth stressing that this rise is a robust result of the pole extrapolation and not a consequence of the renormalization of the data, which in fact decreases somewhat the observed rise. The upward turn at $x > 0.6$ is also observed in the $d(e, e')X$ analysis[71] for up to $x = 0.7$, in which the medium modification effects in the deuteron are estimated using the observed correlation between nuclear EMC and short-range correlation effects. It is worth noting the phenomenological fits of Bosted and Christy[69,70] also show a rise of the F_{2n}/F_{2p} in this x, Q^2 range, albeit not up to the same level as observed in our extraction. As their fits are based on inclusive data, one has to keep in mind that their systematic errors in this kinematic region are also large due to the nuclear effects that need to be taken into account.

Due to the moderate Q^2 values of the experiment, the two highest x points shown in Fig. 8 are at $W \approx 1.18\,\text{GeV}$ corresponding to the kinematics of Δ-resonance electroproduction. Therefore one cannot relate the observed increase of the F_{2n}/F_{2p}

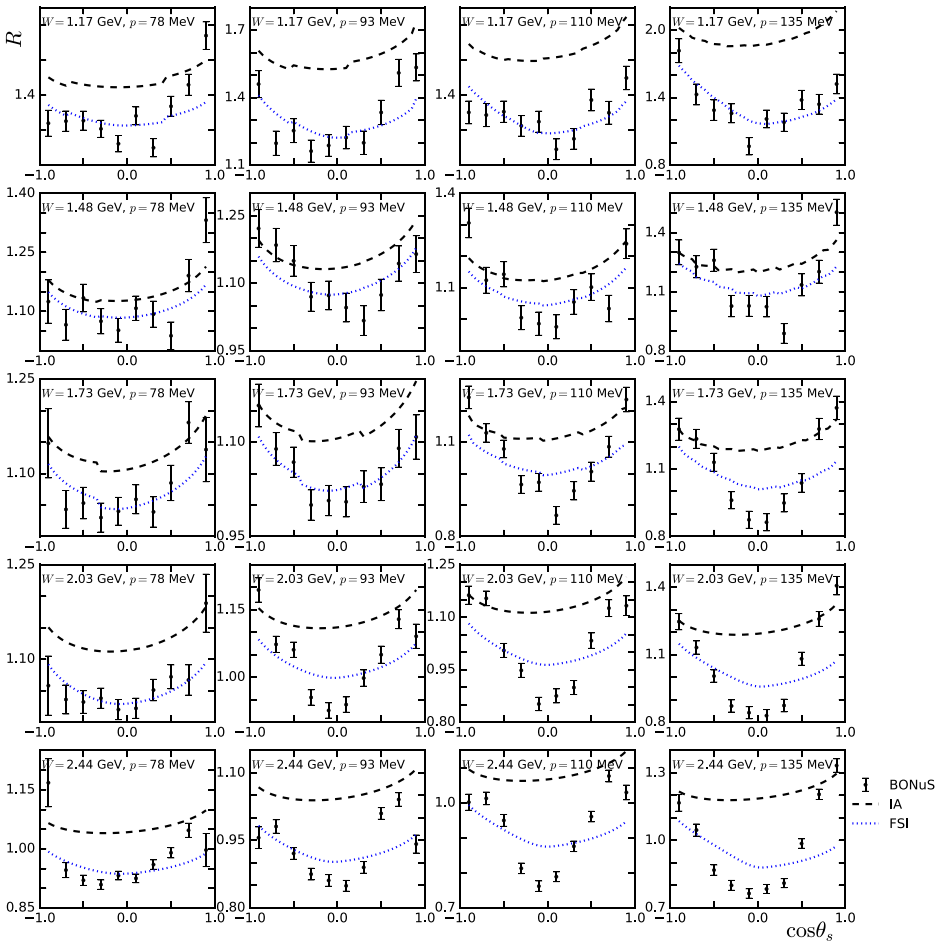

Fig. 7. (Color online) Ratio R of the BONuS data[60] to a plane-wave model as a function of spectator $\cos\theta_s$ compared to VNA IA (black dashed curves) and FSI (dotted blue curves) calculations for $E_{\rm beam} = 5.27\,{\rm GeV}$ and $Q^2 = 1.66\,{\rm GeV}^2$. Normalization factors have been fitted for each p_s values, see text for details. The IA calculations are shown using the same normalization factors.

ratio directly to the u- and d- quark distributions. It will be interesting to see if such a behavior of F_{2n}/F_{2p} persists at higher energies probed by BONuS12.[62]

If the rise would persist in the true DIS region, one possible explanation discussed in Ref. 30 is the presence of a hard isosinglet ud quark correlation in the nucleon at $x \to 1$. Such a correlation will result in a momentum sharing effect similar to one observed recently in asymmetric nuclei in the proton–neutron short range correlation region.[72,73] According to this observation, the short range correlation between unlike components in the asymmetric two-Fermi system will result in the small component's dominance in the correlation region such that

$$f_1 n_1(p) \approx f_2 n_2(p), \tag{25}$$

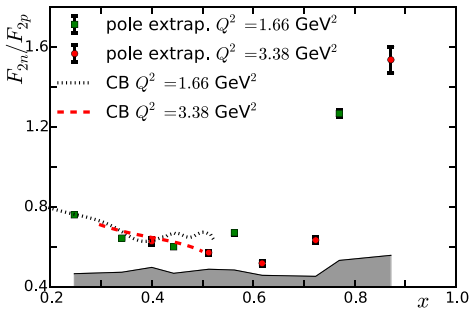

Fig. 8. (Color online) F_{2n} to F_{2p} ratio obtained using the pole extrapolation applied to the renormalized BONuS data. Systematic errors are depicted as the shaded band. The dotted black and dashed red curves show the ratio obtained with F_{2n} parametrization of Ref. 69. The F_{2p} values are estimated using the fit of Ref. 70. Figure adapted from Ref. 30.

where f_i and $n_i(p)$ are the fraction and momentum distribution of the component i in the high momentum region. Here, the $n_i(p)$ are normalized to unity.

If such ud short-range correlations are present in the nucleon, then because of the valence quark distributions being normalized to their relative fractions, Eq. (25) for quark distributions will correspond to

$$u(x) \approx d(x) \tag{26}$$

in the $x \to 1$ limit. Such a relation will result in the rise of the F_{2n}/F_{2p} ratio in the region of x in which the ud correlations are dominant.

5. Final-State Interactions in Inclusive DIS

Scattering effects involving more than one nucleon are known to play a role in inclusive nuclear DIS. At small x, the beam scattering off two or more nucleons gives rise to interference effects that result in shadowing and anti-shadowing corrections.[74–79] Another example is the final-state interactions between hadronic debris of the struck quark and nucleons in the residual nucleus. These FSI effects, however, are routinely assumed to be negligible. This can be justified by the closure approximation at small values of x and large W, in which case the sum over all hadronic degrees of freedom in the final state, unrestricted in phase space, can be expressed through the sum over the noninteracting quark degrees of freedom. This corresponds to the dynamical picture in which the final-state rearrangements of the produced hadrons do not influence the initial state probability distribution of the interacting partons.

The situation is different at high x and moderate values of invariant mass W (or Q^2). In this case, the dynamical picture represents a final hadronic state that contains all the valence quarks originating from the struck nucleon which can reinteract coherently with the nucleons from the residual nucleus (similar to the situation presented in Fig. 1(a)). In these kinematics, due to the restricted phase space in the final state, the quark-hadron duality[80] is not fully satisfied and the closure approximation

cannot be applied. A proper calculation of FSI effects in these kinematics requires detailed knowledge of the composition and distribution of internal degrees of freedom of the final hadronic system, which makes this problem very challenging.

In Ref. 81, we studied inclusive FSI for the deuteron target, based on the above outlined VNA/GEA approximation, using rescattering parameters obtained from the comparison with the *Deeps* data (Sec. 3.2) as an input. The theoretical formalism for computation of the FSI contribution to the inclusive DIS cross-section is based on the application of the optical theorem which allows to relate the hadronic tensor of inclusive nuclear scattering,[b] $W_D^{\mu\nu}$ to the imaginary part of the forward nuclear Compton scattering amplitude $\mathcal{A}^{\mu\nu}_{\gamma^* A}(t=0)$ as follows[81]:

$$W_D^{\mu\nu} = \frac{1}{2\pi M_D}\frac{1}{3}\sum_{\lambda_D} \Im m\, \mathcal{A}^{\mu\nu}_{\gamma^* A}(t=0). \tag{27}$$

Under the same assumptions detailed in Sec. 2.1, the VNA can be applied to the inclusive DIS reaction on the deuteron, and the two diagrams shown in Fig. 9 contribute to the forward Compton amplitude in Eq. (27). The first (IA) term represents the propagation of the state X' resulting from the γ^*–bound nucleon scattering, without interacting with the spectator nucleon in the intermediate state, see Fig. 9(a). The second (rescattering) term describes the production of the hadronic state (X_1) which interacts with the spectator nucleon (S_1) in the intermediate state, see Fig. 9(b). In this diagram one sums over the all intermediate X_1 and X_2 states. This diagram is responsible for the FSI contribution to the inclusive cross-section

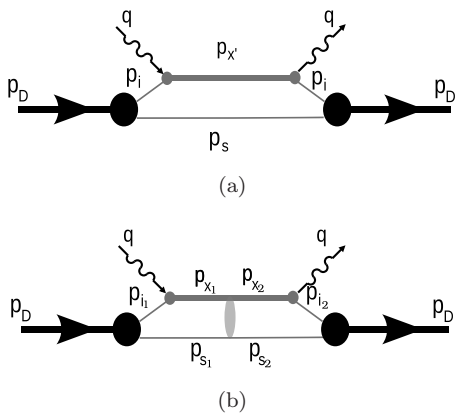

Fig. 9. Forward virtual Compton scattering amplitude for the deuteron, comprising of (a) the Born diagram, and (b) the rescattering contribution. The gray blob in the intermediate state represents the effective interaction between the hadronic debris (X_1) and spectator nucleon (S_1) resulting in the production of the final hadronic state (X_2) and nucleon (S_2). The deuteron momentum in the Born diagram is given by $p_D = p_i + p_s$, and in the FSI diagram by $p_D = p_{i_1} + p_{s_1} = p_{i_2} + p_{s_2}$. Figure adapted from Ref. 81.

[b]All hadronic tensors refer to the inclusive process in this section.

through relation (27). It can be calculated within the GEA in which case all higher order rescattering contributions are included in the effective rescattering vertex.

The plane-wave IA diagram (Fig. 9(a)) results in the standard convolution formula[81]

$$W_D^{\mu\nu(\mathrm{pw})} = \frac{2m_N}{M_D}\sum_N \int d^3\boldsymbol{p}_s\, W_N^{\mu\nu}\, S(p_s), \tag{28}$$

where the sum is over the nucleons $N = p, n$ and the undistorted momentum distribution $S(p_s)$ is given by the first term in Eq. (19).

To apply the GEA to the FSI diagram (Fig. 9(b)) two conditions must be met: (i) the intermediate state X_1 can be characterized by an effective hadronic state whose interactions with the spectator nucleon are similar to hN interactions (minimal Fock component picture); (ii) the produced effective state has high enough momentum to apply the eikonal approximation within the GEA. The second condition restricts the x range for intermediate states with an invariant mass $W > 2\,\mathrm{GeV}$ at $Q^2 \lesssim 5\,\mathrm{GeV}^2$.[81] In the calculation of the FSI diagram, the zero-component integrations of the momenta in the loops are used to put the spectator nucleon on its mass shell before and after the FSI. As in the semi-inclusive case (Sec. 3.1) the integrations over the z-component of the two loop momenta will result in two FSI contributions corresponding to on- and off- shell intermediate X_1, X_2 states. The final result for these two contributions is[81]:

$$\begin{aligned} W_{\mathrm{FSI}}^{\mu\nu(\mathrm{on})} = &-\sum_N \frac{2m_N}{M_D}\int d^3\boldsymbol{p}_{s_1}\frac{W_N^{\mu\nu}(p_{i_1},q,m_{X_1})}{8\sqrt{E_{s_1}}}\frac{1}{3}\sum_{X_2}\sum_{\sigma_i,\sigma_s,\lambda_D}\int\frac{d^2\boldsymbol{p}_{s_2,\perp}}{(2\pi)^2} \\ &\times \Im m\left\{\frac{\beta(s_{XN},m_{X_1})f^{(\mathrm{on})}_{N\{X_1\},NX_2}(t_{XN})}{\left||\boldsymbol{q}|-(M_D+q^0)\widetilde{p}^{X_2}_{s_2,z}/\widetilde{E}_{s_2}\right|\sqrt{\widetilde{E}_{s_2}}}\right. \\ &\left.\times\,\Psi_D^{\lambda_D\dagger}(\widetilde{p}^{X_2}_{i_2},\sigma_i;\widetilde{p}^{X_2}_{s_2},\sigma_s)\Psi_D^{\lambda_D}(p_{i_1},\sigma_i;p_{s_1},\sigma_s)\right\}, \end{aligned} \tag{29}$$

$$\begin{aligned} W_{\mathrm{FSI}}^{\mu\nu(\mathrm{off})} = &\sum_{N,X_2}\frac{2m_N}{M_D}\int dW\,W\int d^2\boldsymbol{p}_{s_{1,\perp}}\widetilde{p}^{X_2}_{s_{1,z}}\frac{W_N^{\mu\nu(\mathrm{off})}(\tilde{p}^{X_2}_{i_1},q,W)}{8\left||\boldsymbol{q}|-(M_D+q^0)\,\widetilde{p}^{X_2}_{s_1,z}/\widetilde{E}_{s_1}\right|\sqrt{\widetilde{E}_{s_1}}} \\ &\times\frac{1}{3}\sum_{\sigma_i,\sigma_s,\lambda_D}\int\frac{d^2\boldsymbol{p}_{s_2,\perp}}{(2\pi)^2}\tilde{p}^{X_2}_{s_2,z}\,\Im m\left\{\frac{\beta(s_{XN},W)f^{(\mathrm{off})}_{N\{X_1\}_W,NX_2}(t_{XN})}{\left||\boldsymbol{q}|-(M_D+q^0)\,\widetilde{p}^{X_2}_{s_2,z}/\widetilde{E}_{s_2}\right|\sqrt{\widetilde{E}_{s_2}}}\right. \\ &\left.\times\,\widetilde{\Psi}_D^{\lambda_D\dagger}(\widetilde{p}^{X_2}_{i_1},\sigma_i;\widetilde{p}^{X_2}_{s_1},\sigma_s)\widetilde{\Psi}_D^{\lambda_D}(\widetilde{p}^{X_2}_{i_2},\sigma_i;\widetilde{p}^{X_2}_{s_2},\sigma_s)\right\}. \end{aligned} \tag{30}$$

Here, the four-vectors are $\widetilde{p}^{X_2}_{s_2} = (\widetilde{E}_{s_2}; \boldsymbol{p}_{s_2,\perp}, \widetilde{p}^{X_2}_{s_2,z})$ and $\widetilde{p}^{X_2}_{i_2} = p_D - \widetilde{p}^{X_2}_{s_2}$, with $\{X_{1/2}\}$ denoting intermediate states with $p^2_{X_{1/2}} = m^2_{X_{1/2}}$. The longitudinal component of $\widetilde{p}^{X_2}_{s_2}$ is defined from the relation:

$$2|\boldsymbol{q}|\,\widetilde{p}^{X_2}_{s_2,z} - 2(M_D + q^0)\widetilde{E}_{s_2} = m^2_{X_2} - M^2_D + Q^2 - 2M_D q^0 - m^2_N, \tag{31}$$

where $\widetilde{E}_{s_2} = \sqrt{m^2_N + \boldsymbol{p}^2_{s_2,\perp} + (\widetilde{p}^{X_2}_{s_2,z})^2}$. The detailed expressions for nucleon hadronic tensors, $W^{\mu\nu}_N$, $W^{\mu\nu(\text{off})}_N$, rescattering amplitudes $f^{(\text{on})}_{N\{X_1\},NX_2}$, $f^{(\text{off})}_{N\{X_1\}_W,NX_2}$, as well as distorted deuteron wave function, $\widetilde{\Psi}^{\lambda_D\dagger}_D$ appearing in Eq. (30) can be found in Ref. 26.

In Eqs. (29) and (30), the momentum fraction of the partons absorbing and emitting the virtual photon, obeys the constraints:

$$x_1 = \frac{Q^2}{2p_{i_1}\cdot q} < 1, \quad x_2 = \frac{Q^2}{2p_{i_2}\cdot q} < 1. \tag{32}$$

These impose an additional restriction on the phase space of the loop integrations in Eqs. (29) and (30). Rewriting

$$x_2 = \frac{1}{1 + (m^2_{X_2} - (\tilde{p}^{X_2}_{i_2})^2)/Q^2} \approx \frac{1}{1 + (m^2_{X_2} - m^2_N)/Q^2}, \tag{33}$$

one observes that for any fixed value of m_{X_2}, the FSI terms are suppressed kinematically in the high Q^2 limit which results in $x_2 \to 1$.

To perform practical calculations of Eqs. (29) and (30) one needs to model the spectrum of available intermediate states. In Ref. 81 this spectrum was modeled by considering three effective resonance contributions with $m_X = 1.232, 1.5$ and $1.75\,\text{GeV}$. Such a choice of the masses allows to account for the FSI contributions from the Δ-isobar, and the first and second resonance regions. It was assumed that all these contributions are in phase thus providing the maximum possible FSI contribution to the cross-section. Additionally, for higher W the distribution in M_X with a certain width has been added to the intermediate state spectrum to account for FSI contributions that cannot be characterized by an effective resonance. Finally, the parameters entering the rescattering amplitudes $f^{(\text{on})}$ and $f^{(\text{off})}$ were taken from the results of the comparison with the *Deeps* data discussed in Sec. 3.2.[81]

To illustrate the FSI effects in the inclusive scattering, we show calculations of the inclusive structure function F_2, which is related to the semi-inclusive structure functions of Eq. (15) in the following way:

$$F^D_2 = \sum_N \int \frac{d^3\boldsymbol{p}_s}{(2\pi)^2 2E_s}\left[F_L(Q^2, \tilde{x}, \boldsymbol{p}_s) + \frac{x}{\gamma^2}F_T(Q^2, \tilde{x}, \boldsymbol{p}_s)\right], \tag{34}$$

where $\gamma = \boldsymbol{q}^2/q_0^2 = 1 + 4x^2m^2_N/Q^2$.

Figure 10 shows the ratio of F^D_2 including the FSI effects to the plane-wave IA calculation for four different values of Q^2. The calculations were performed with the SLAC parametrization for nucleon structure functions,[82] which cover a wide range

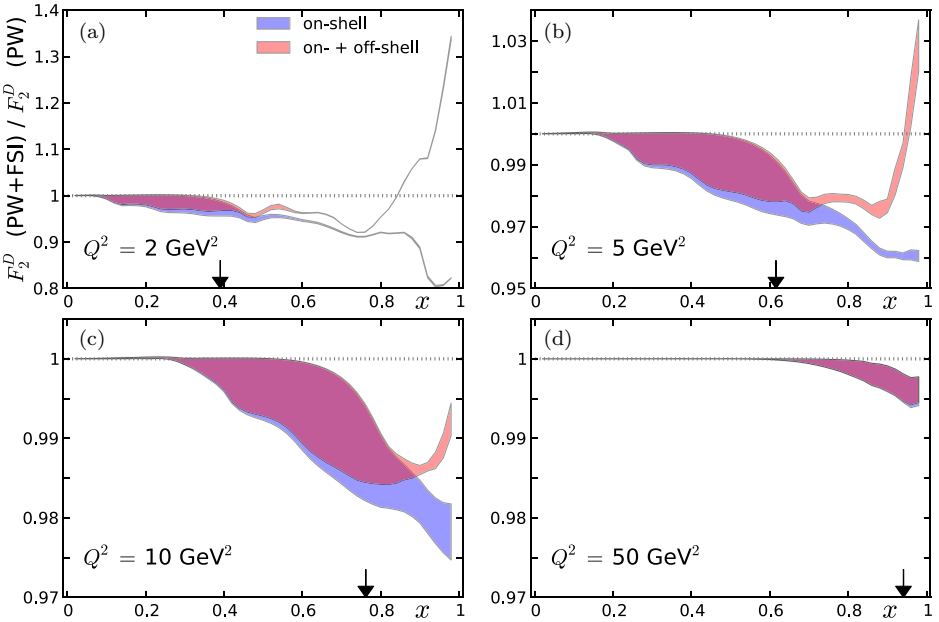

Fig. 10. (Color online) Ratio of the deuteron F_2^D structure function including FSIs to that computed in the plane-wave (PW) approximation, at several values of Q^2 from 2 GeV^2 to 50 GeV^2. The on-shell only results from Eq. (29) (blue shaded bands) and those including off-shell contributions from Eq. (30) (pink shaded bands) span the range of models for the distribution of intermediate state masses (see Ref. 81 for details). The arrows along the x-axis indicate the $W = 2$ GeV point at each Q^2 value for free nucleon kinematics. Figure adapted from Ref. 81.

of Q^2 and invariant mass W, and with the deuteron wave function based on the Paris potential.[83] Here, the bands envelope the range of intermediate state mass distributions described above with the upper bound excluding the distribution in M_{X_2} contribution above the resonance region, and the lower bound including it. The general observation arising from these calculations is that FSI effects are largest at low Q^2 values and $x \to 1$. This corresponds to the kinematic region where the intermediate states in the FSI have the largest available phase space to contribute in Eqs. (29) and (30), also see Eq. (32). The on-shell part of the FSI (Eq. (29)) diminishes F_2^D with the largest reduction of $\sim 20\%$ occurring at $Q^2 = 2$ GeV^2 and $x \gtrsim 0.9$. The off-shell contribution of Eq. (30) has the opposite effect, increasing F_2^D again. The overall FSI effect is quite small at low and moderate values of x but becomes large at low Q^2 and high values of x.

6. Final-State Interaction Effects in DIS From Tensor Polarized Deuteron

As the deuteron is a spin 1 target, it can be prepared in a tensor polarized state and additional structure functions will appear in the cross-section compared to the spin 1/2 nucleon case. In inclusive DIS these are the four structure functions

b_{1-4},[84] where b_1 and b_2 are leading twist and obey a Callan–Gross-like relation in the Bjorken scaling limit. Moreover b_1 has an explicit interpretation in the parton model which relates it to the distribution of unpolarized quarks in a polarized nucleus

$$b_1 = \frac{1}{2}\sum_q e_q^2(q^0 - q^1), \tag{35}$$

where q^i represents the quark distribution function in a deuteron with polarization i. As such b_1 presents an object where quark and nuclear degrees of freedom are inherently interconnected. In DIS with an unpolarized lepton beam and a polarized deuteron target, the measured tensor asymmetry

$$A_{zz} = \frac{\sigma^+ + \sigma^- - 2\sigma^0}{\sigma^+ + \sigma^- + \sigma^0}, \tag{36}$$

where σ^i denotes the cross-section with deuteron polarization i, can be related to the b_1 structure function. For the deuteron considered as a two-nucleon interacting system, b_1 is only nonzero due to the partial D-wave admixture.[85] As such it could provide a new framework for probing orbital angular effects in QCD[86] in addition to the spin-1/2 nucleon which is being studied intensively.

Because of the smallness of the D component in the deuteron, the expectation is that b_1 should be small in the conventional IA picture of scattering. There are several effects beyond IA which have been observed theoretically to contribute to the structure function b_1. At low x, the shadowing corrections are expected to contribute to b_1.[87–90] Also, it was observed in Ref. 91 that nonnucleonic components in the deuteron such as pionic and hidden color components can provide a sizeable contribution to b_1.

The A_{zz} tensor asymmetry was measured by the Hermes collaboration[92] for $0.01 < x < 0.45$ at $0.5 < Q^2 < 5\,\mathrm{GeV}^2$, finding nonzero values which exhibit a sign change around $x \approx 0.3$. Currently no conventional nuclear physics model can explain the Hermes data, though higher twist effects, not accounted for in the analysis of Ref. 92, could possibly play a role.[93,94] In the near future, two experiments at Jefferson Lab will measure the A_{zz} asymmetry, one at $x < 1$ in the deep inelastic region, and the other at $x > 1$ in quasi-elastic kinematics .[95]

Beyond the IA, another possible contribution to b_1 originates from the nuclear FSI between produced hadrons and the nuclear medium. In Ref. 96, the effect of these FSIs in the generation of the tensor asymmetry A_{zz} has been estimated for the resonance region with the model outlined in Sec. 5. Again, the two diagrams presented in Fig. 9 have been taken into account, but now with a tensor polarized deuteron. For the nominator in Eq. (36) one needs to calculate:

$$W_D^{\mu\nu(\mathrm{tensor})} = \rho_{\lambda\lambda'}[W_D^{\mu\nu(\mathrm{pw})}(\lambda',\lambda) + W_{\mathrm{FSI}}^{\mu\nu(\mathrm{on})}(\lambda',\lambda) + W_{\mathrm{FSI}}^{\mu\nu(\mathrm{off})}(\lambda',\lambda)] \tag{37}$$

with deuteron density matrix

$$\rho_{\lambda\lambda'} = \frac{1}{3}\mathrm{diag}(1,-2,1), \tag{38}$$

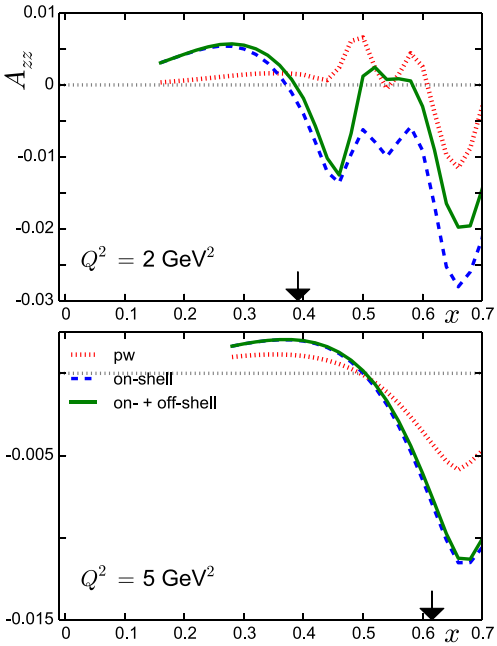

Fig. 11. (Color online) Tensor asymmetry A_{zz} for kinematics accessible in the upcoming JLab experiment[95] (incoming beam of 11 GeV). The red dotted curves show the plane-wave IA calculations, the blue dashed (green full) curves include the on-shell (and off-shell) FSI contributions. For details on the FSI on- and off-shell calculations, we refer to Ref. 81. Deuteron polarization is along the virtual photon axis. The arrow along the x-axis indicates the boundary at $W = 2$ GeV between the resonance and DIS regions for free nucleon kinematics. Figure adapted from Ref. 96.

where λ (λ') are the polarization of the initial (final) state deuteron in the forward Compton scattering amplitude. Because of the diffractive regime of FSI only the helicity conserving part of the rescattering amplitude is included in the calculations. The set of possible intermediate states include the three resonance contributions discussed in Sec. 5.

Figure 11 shows the results of these estimates for kinematics covered in the JLab proposal aiming at the extraction of b_1 at $x < 1$. For the plane-wave calculations, we observe that A_{zz} is almost zero for Bjorken x in the DIS region, while it reaches values of the order of $\sim \pm 0.01$ in the resonance region at $Q^2 = 2\,\text{GeV}^2$ and becomes smaller with increasing Q^2. Adding the FSI contributions has a significant effect on the size of A_{zz} over the entire x range. At $Q^2 = 2\,\text{GeV}^2$, the off-shell part of the FSI diagram also has a sizable contribution while at $Q^2 = 5\,\text{GeV}^2$ it is almost negligible. It is worth mentioning that even though the effective hadronic states taken into account in the FSI diagram all lie in the resonance region, they also contribute significantly to A_{zz} in the DIS region. This can be understood in the following manner. In the formalism A_{zz} is only nonzero because of the D-wave component of the deuteron wave function, both in the plane-wave and FSI contribution to

the cross-section. As the dominant contribution for the D-wave occurs at momenta above 250 MeV, A_{zz} measured in the DIS region is still sensitive to the resonance region of FSI. This is due to the fact that at large Fermi momenta, the produced mass in the intermediate state in Fig. 9(b) can be smaller than the mass computed for the stationary nucleon at the same Bjorken x. Comparing our calculation at the largest $x = 0.45$ ($\langle Q^2 \rangle \approx 5\,\mathrm{GeV}^2$) measured by Hermes, we obtain a value of $A_{zz} \approx 0.0015$, which is about two orders of magnitude smaller than the experimental value, $A_{zz}^{\mathrm{exp}} = 0.157 \pm 0.69$. Consequently, the inclusion of nuclear FSI is not enough to explain the size of the measured Hermes asymmetry.

7. Conclusions and Outlook

In the present work, we reviewed recent studies of FSI processes in deep inelastic scattering involving a deuteron target. FSIs provide an additional venue in exploring the QCD dynamics in a way which is complementary to more conventional approaches. We demonstrate that focusing on the kinematics in which FSI is dominant in semi-inclusive DIS off the deuteron with a tagged spectator (reaction (4)), gives a completely new tool in the investigation of the structure of DIS final states and the process of QCD hadronization. Another direction in studies of semi-inclusive processes involving the deuteron is the possibility of performing pole extrapolation in the extraction of "free" structure functions of the bound nucleon. The FSI effects are also important for inclusive processes especially when the quantities under the investigation are small, such as medium modification effects in the deuteron or probing tensor-polarized structure functions in the deuteron.

We investigated these processes within the framework of virtual nucleon approximation in which FSI is treated based on the generalized eikonal approximation. Both approximations require special conditions for the DIS kinematics such as the deuteron wave function being dominated by the pn component and the coherent outgoing final states undergoing diffractive-like rescattering.

The presented theoretical framework allows several extensions both in considering new processes and new kinematical domains in DIS:

- The method can be extended to more complex nuclei ($A \geq 3$) and with more complex nuclear spectator states: $A-1$ coherent spectator system, N-body breakup, etc. For inclusive scattering it will be interesting to investigate at which level the FSI can produce an EMC-like effect at $x > 0.8$. As the mechanism is dominated by small distances, the first rescattering will dominate in large nuclei and Q^2-dependence is expected to cancel in ratios of F_A/F_D. This needs to be quantified, however, by explicit model calculations.
- The influence of nuclear final-state interactions can be studied in more exclusive nuclear DIS reactions. For instance double virtual Compton scattering on nuclei (coherent and incoherent). The data already exist from the Hermes collaboration[97] and the new CLAS collaboration data are currently being analyzed.[98] Another possibility is the detection of hadrons originating from the current

fragmentation region, both with or without detection of spectator nuclear fragments. Such semi-inclusive DIS reactions on light nuclei can be used in the determination of neutron transverse momentum distributions.[99] One important issue to consider is the possible interplay between nuclear and partonic FSIs with the latter[100,101] generating nonzero single-spin asymmetries on proton targets.

- Besides semi-inclusive experiments off the deuteron at 12 GeV JLab,[62,63] the scope of the FSI studies can be extended to the semi-inclusive processes currently being considered for an electron-ion collider (EIC).[102,103] The tagged spectator process is experimentally better suited for collider kinematics, especially for measurements with very low spectator momenta (relative to the nucleus center of mass). In deuteron DIS in the EIC setup, the spectator nucleon is produced in the target fragmentation region with approximately half the deuteron beam momentum and can be detected with forward detectors. This is much more advantageous than in a fixed target setup in which case a dedicated recoil detector is needed to detect spectator nucleons at small momenta. Additionally in the currently discussed EIC designs a possibility of polarized deuteron or ^{3}He beams[104–106] are being considered. The semi-inclusive DIS processes with polarized ion beams will allow the extraction of on-shell nucleon spin structure functions through the pole extrapolation method outlined in Sec. 4. An R&D project is currently developing the theoretical and experimental tools for assessing the potential of such measurements.[107–109] As the x and Q^2 coverage of the EIC design corresponds to the nuclear FSI whose dynamics are dominated by the Feynman mechanism Fig. 1(b), the GEA framework cannot be applied here, and new theoretical approaches need to be developed.[110]
- Finally, one can extend the GEA framework discussed in the review to account for spin flip effects in the FSI processes. The consideration of such effects in the FSI is especially important for studies involving polarized deuteron targets (see Sec. 6) as well as processes involving the measurement of different asymmetries in polarized electron — polarized target DIS.

Overall, the upcoming 12 GeV experiments at Jefferson Lab and the discussed experimental possibilities at an EIC provide a multitude of new opportunities for investigation of the dynamics of final-state interactions in deep-inelastic processes. Such studies have significant potential in advancing our understanding of the QCD dynamics of the DIS final state and its hadronization.

Acknowledgments

We are thankful to our colleagues, Drs. Vadim Guzey, Charles Hyde, Sebastian Kuhn, Shunzo Kumano, Pawel Nadel-Turonski, Kijun Park, Mark Strikman and Christian Weiss for numerous discussions on useful comments on the physics of semi-inclusive DIS processes. This work is supported by the U.S. Department of Energy Grant under Contract DE-FG02-01ER41172.

References

1. J. D. Bjorken, *Lect. Notes Phys.* **56** (1976) 93.
2. L. L. Frankfurt and M. I. Strikman, *Phys. Rep.* **160** (1988) 235.
3. L. Frankfurt, M. Sargsian and M. Strikman, *Int. J. Mod. Phys. A* **23** (2008) 2991, arXiv:0806.4412 [nucl-th].
4. M. M. Sargsian, T. V. Abrahamyan, M. I. Strikman and L. L. Frankfurt, *Phys. Rev. C* **71** (2005) 044614, arXiv:nucl-th/0406020 [nucl-th].
5. M. M. Sargsian, T. V. Abrahamyan, M. I. Strikman and L. L. Frankfurt, *Phys. Rev. C* **71** (2005) 044615, arXiv:nucl-th/0501018 [nucl-th].
6. G. P. Lepage and S. J. Brodsky, *Phys. Rev. D* **22** (1980) 2157.
7. A. H. Mueller, *Phys. Rep.* **73** (1981) 237.
8. L. Frankfurt, W. R. Greenberg, G. A. Miller and M. Strikman, *Phys. Rev. C* **46** (1992) 2547, arXiv:nucl-th/9211002 [nucl-th].
9. R. P. Feynman, *Photon-Hadron Interactions* (Avaion Publishing, US, 1973).
10. W. Cosyn, V. Guzey, M. Sargsian, M. Strikman and C. Weiss, *EPJ Web Conf.* **112** (2016) 01022, arXiv:1601.06665 [hep-ph].
11. L. S. Osborne, C. Bolon, R. L. Lanza, D. Luckey, D. G. Roth, J. F. Martin, G. J. Feldman, M. E. B. Franklin, G. Hanson and M. L. Perl, *Phys. Rev. Lett.* **40** (1978) 1624.
12. European Muon Collab. (J. Ashman *et al.*), *Z. Phys. C* **52** (1991) 1.
13. HERMES Collab. (A. Airapetian *et al.*), *Phys. Lett. B* **577** (2003) 37, arXiv:hep-ex/0307023 [hep-ex].
14. HERMES Collab. (A. Airapetian *et al.*), *Nucl. Phys. B* **780** (2007) 1, arXiv:0704.3270 [hep-ex].
15. K. Hafidi, *AIP Conf. Proc.* **870** (2006) 669, arXiv:nucl-ex/0609005 [nucl-ex].
16. BRAHMS Collab. (I. Arsene *et al.*), *Phys. Rev. Lett.* **93** (2004) 242303, arXiv:nucl-ex/0403005 [nucl-ex].
17. BRAHMS Collab. (I. Arsene *et al.*), *Nucl. Phys. A* **757** (2005) 1, arXiv:nucl-ex/0410020 [nucl-ex].
18. STAR Collab. (J. Adams *et al.*), *Nucl. Phys. A* **757** (2005) 102, arXiv:nucl-ex/0501009 [nucl-ex].
19. B. Z. Kopeliovich, J. Nemchik, E. Predazzi and A. Hayashigaki, *Nucl. Phys. A* **740** (2004) 211, arXiv:hep-ph/0311220 [hep-ph].
20. M. Gyulassy and M. Plumer, *Nucl. Phys. B* **346** (1990) 1.
21. E. Wang and X.-N. Wang, *Phys. Rev. Lett.* **89** (2002) 162301, arXiv:hep-ph/0202105 [hep-ph].
22. A. Accardi, *Eur. Phys. J. C* **49** (2007) 347, arXiv:nucl-th/0609010 [nucl-th].
23. L. Lapikas, G. van der Steenhoven, L. Frankfurt, M. Strikman and M. Zhalov, *Phys. Rev. C* **61** (2000) 064325, arXiv:nucl-ex/9905009 [nucl-ex].
24. V. R. Pandharipande and S. C. Pieper, *Phys. Rev. C* **45** (1992) 791.
25. L. L. Frankfurt, E. J. Moniz, M. M. Sargsian and M. I. Strikman, *Phys. Rev. C* **51** (1995) 3435, arXiv:nucl-th/9501019 [nucl-th].
26. W. Cosyn and M. Sargsian, *Phys. Rev. C* **84** (2011) 014601, arXiv:1012.0293 [nucl-th].
27. G. R. Farrar, H. Liu, L. L. Frankfurt and M. I. Strikman, *Phys. Rev. Lett.* **61** (1988) 686.
28. M. Sargsian and M. Strikman, *Phys. Lett. B* **639** (2006) 223, arXiv:hep-ph/0511054.
29. CLAS Collab. (N. Baillie *et al.*), *Phys. Rev. Lett.* **108** (2012) 199902, arXiv:1110.2770 [nucl-ex].

30. W. Cosyn and M. M. Sargsian, *Phys. Rev. C* **93** (2016) 055205, arXiv:1506.01067 [hep-ph].
31. W. Melnitchouk, M. Sargsian and M. I. Strikman, *Z. Phys. A* **359** (1997) 99, arXiv:nucl-th/9609048 [nucl-th].
32. C. Ciofi degli Atti, L. L. Frankfurt, L. P. Kaptari and M. I. Strikman, *Phys. Rev. C* **76** (2007) 055206, arXiv:0706.2937 [nucl-th].
33. R. B. Wiringa, V. G. J. Stoks and R. Schiavilla, *Phys. Rev. C* **51** (1995) 38, arXiv:nucl-th/9408016 [nucl-th].
34. R. Machleidt, *Phys. Rev. C* **63** (2001) 024001, arXiv:nucl-th/0006014 [nucl-th].
35. CLAS Collab. (K. S. Egiyan *et al.*), *Phys. Rev. Lett.* **98** (2007) 262502, arXiv:nucl-ex/0701013 [nucl-ex].
36. Hall A Collab. (W. U. Boeglin *et al.*), *Phys. Rev. Lett.* **107** (2011) 262501, arXiv:1106.0275 [nucl-ex].
37. W. Boeglin and M. Sargsian, *Int. J. Mod. Phys. E* **24** (2015) 1530003, arXiv:1501.05377 [nucl-ex].
38. C. Ciofi degli Atti and S. Liuti, *Phys. Rev. C* **41** (1990) 1100.
39. M. M. Sargsian, S. Simula and M. I. Strikman, *Phys. Rev. C* **66** (2002) 024001, arXiv:nucl-th/0105052 [nucl-th].
40. M. Hirai, S. Kumano, K. Saito and T. Watanabe, *Phys. Rev. C* **83** (2011) 035202, arXiv:1008.1313 [hep-ph].
41. S. A. Kulagin and R. Petti, *Nucl. Phys. A* **765** (2006) 126, arXiv:hep-ph/0412425 [hep-ph].
42. C. Ciofi degli Atti, L. P. Kaptari and S. Scopetta, *Eur. Phys. J. A* **5** (1999) 191, arXiv:hep-ph/9904486.
43. C. Ciofi degli Atti and B. Z. Kopeliovich, *Eur. Phys. J. A* **17** (2003) 133, arXiv:nucl-th/0207001.
44. C. Ciofi degli Atti, L. P. Kaptari and B. Z. Kopeliovich, *Eur. Phys. J. A* **19** (2004) 145, arXiv:nucl-th/0307052.
45. V. Palli, C. Ciofi degli Atti, L. P. Kaptari, C. B. Mezzetti and M. Alvioli, *Phys. Rev. C* **80** (2009) 054610, arXiv:0911.1377 [nucl-th].
46. C. Ciofi degli Atti and L. P. Kaptari, *Phys. Rev. C* **83** (2011) 044602, arXiv:1011.5960 [nucl-th].
47. L. L. Frankfurt, M. M. Sargsian and M. I. Strikman, *Phys. Rev. C* **56** (1997) 1124, arXiv:nucl-th/9603018.
48. M. M. Sargsian, *Int. J. Mod. Phys. E* **10** (2001) 405, arXiv:nucl-th/0110053.
49. L. L. Frankfurt, W. R. Greenberg, G. A. Miller, M. M. Sargsian and M. I. Strikman, *Z. Phys. A* **352** (1995) 97, arXiv:nucl-th/9501009 [nucl-th].
50. L. Frankfurt, E. Piasetsky, M. Sargsian and M. Strikman, *Phys. Rev. C* **51** (1995) 890, arXiv:nucl-th/9405003 [nucl-th].
51. M. M. Sargsian, *Phys. Rev. C* **82** (2010) 014612, arXiv:0910.2016 [nucl-th].
52. L. Frankfurt, W. Koepf, J. Mutzbauer, G. Piller, M. Sargsian and M. Strikman, *Nucl. Phys. A* **622** (1997) 511, arXiv:hep-ph/9703399 [hep-ph].
53. L. Frankfurt, M. Strikman, G. Piller and M. Sargsian, *Nucl. Phys. A* **631** (1998) 502C.
54. A. J. Freese and M. M. Sargsian, *Phys. Rev. C* **88** (2013) 044604, arXiv:1306.2368 [nucl-th].
55. L. Frankfurt, M. Johnson, M. Sargsian, W. Weise and M. Strikman, *Phys. Rev. C* **60** (1999) 055202, arXiv:nucl-th/9808016 [nucl-th].
56. O. Artiles and M. M. Sargsian, *Phys. Rev. C* **94** (2016) 064318, arXiv:1606.00468 [nucl-th].

57. F. Gross, *Phys. Rev. C* **26** (1982) 2203.
58. L. L. Frankfurt and M. I. Strikman, *Phys. Lett. B* **64** (1976) 433.
59. CLAS Collab. (A. V. Klimenko *et al.*), *Phys. Rev. C* **73** (2006) 035212, arXiv:nucl-ex/0510032.
60. CLAS Collab. (S. Tkachenko *et al.*), *Phys. Rev. C* **89** (2014) 045206, arXiv:1402.2477 [nucl-ex], Addendum **90** (2014) 059901.
61. I. Niculescu *et al.*, *Phys. Rev. C* **91** (2015) 055206, arXiv:1501.02203 [hep-ex].
62. S. Bueltmann, M. Christy, H. Fenker, K. Griffioen, C. Keppel, S. Kuhn, W. Melnitchouk and V. Tvaskis, JLab Experiment E12-06-113. Available at: http://www.jlab.org/exp_prog/12GEV_EXP/E1206113.html (2006).
63. O. Hen, L. B. Weinstein, S. Gilad and S. A. Wood, arXiv:1409.1717 [nucl-ex].
64. O. Hen, H. Hakobyan, E. Piasetzky and L. Weinstein, Available at: https://www.jlab.org/exp_prog/proposals/15/E12-11-003A.pdf (2015).
65. D. Dutta, K. Hafidi and M. Strikman, *Prog. Part. Nucl. Phys.* **69** (2013) 1, arXiv:1211.2826 [nucl-th].
66. J. Arrington, J. G. Rubin and W. Melnitchouk, *Phys. Rev. Lett.* **108** (2012) 252001, arXiv:1110.3362 [hep-ph].
67. W. Cosyn and M. Sargsian, *AIP Conf. Proc.* **1369** (2011) 121, arXiv:1101.1258 [nucl-th].
68. G. F. Chew and F. E. Low, *Phys. Rev.* **113** (1959) 1640.
69. P. E. Bosted and M. E. Christy, *Phys. Rev. C* **77** (2008) 065206, arXiv:0711.0159 [hep-ph].
70. M. Christy and P. E. Bosted, *Phys. Rev. C* **81** (2010) 055213, arXiv:0712.3731 [hep-ph].
71. L. B. Weinstein, E. Piasetzky, D. W. Higinbotham, J. Gomez, O. Hen and R. Shneor, *Phys. Rev. Lett.* **106** (2011) 052301, arXiv:1009.5666 [hep-ph].
72. M. M. Sargsian, *Phys. Rev. C* **89** (2014) 034305, arXiv:1210.3280 [nucl-th].
73. O. Hen *et al.*, *Science* **346** (2014) 614, arXiv:1412.0138 [nucl-ex].
74. L. Frankfurt and M. Strikman, *Nucl. Phys. B* **316** (1989) 340.
75. N. N. Nikolaev and B. G. Zakharov, *Z. Phys. C* **49** (1991) 607.
76. V. R. Zoller, *Z. Phys. C* **54** (1992) 425.
77. B. Badelek and J. Kwiecinski, *Nucl. Phys. B* **370** (1992) 278.
78. W. Melnitchouk and A. W. Thomas, *Phys. Rev. D* **47** (1993) 3783.
79. G. Piller and W. Weise, *Phys. Rep.* **330** (2000) 1.
80. W. Melnitchouk, R. Ent and C. E. Keppel, *Phys. Rep.* **406** (2005) 127.
81. W. Cosyn, W. Melnitchouk and M. Sargsian, *Phys. Rev. C* **89** (2014) 014612, arXiv:1311.3550 [nucl-th].
82. A. Bodek *et al.*, *Phys. Rev. D* **20** (1979) 1471.
83. M. Lacombe *et al.*, *Phys. Rev. C* **21** (1980) 861.
84. P. Hoodbhoy, R. Jaffe and A. Manohar, *Nucl. Phys. B* **312** (1989) 571.
85. H. Khan and P. Hoodbhoy, *Phys. Rev. C* **44** (1991) 1219.
86. S. Kumano, *Phys. Rev. D* **82** (2010) 017501, arXiv:1005.4524 [hep-ph].
87. L. L. Frankfurt and M. I. Strikman, *Nucl. Phys. A* **405** (1983) 557.
88. N. N. Nikolaev and W. Schafer, *Phys. Lett. B* **398** (1997) 245, arXiv:hep-ph/9611460 [hep-ph].
89. J. Edelmann, G. Piller and W. Weise, *Z. Phys. A* **357** (1997) 129, arXiv:nucl-th/9701026 [nucl-th].
90. K. Bora and R. Jaffe, *Phys. Rev. D* **57** (1998) 6906, arXiv:hep-ph/9711323 [hep-ph].
91. G. A. Miller, *Phys. Rev. C* **89** (2014) 045203, arXiv:1311.4561 [nucl-th].

92. HERMES Collab. (A. Airapetian *et al.*), *Phys. Rev. Lett.* **95** (2005) 242001, arXiv:hep-ex/0506018 [hep-ex].
93. W. Cosyn, Y.-B. Dong, S. Kumano and M. Sargsian, arXiv:1702.05337 [hep-ph].
94. W. Cosyn, Y.-B. Dong, S. Kumano and M. Sargsian, Tensor-polarized structure function b_1 by convolution picture for deuteron, in *22nd Int. Symp. on Spin Physics (SPIN 2016) Urbana, IL, USA, 25–30 September, 2016*, (2017), arXiv:1702.07594 [hep-ph].
95. K. Slifer and E. Long, *PoS* **PSTP2013** (2014) 008, arXiv:1311.4835 [nucl-ex].
96. W. Cosyn and M. Sargsian, *J. Phys. Conf. Ser.* **543** (2014) 012006, arXiv:1407.1653 [nucl-th].
97. HERMES Collab. (A. Airapetian *et al.*), *Phys. Rev. C* **81** (2010) 035202, arXiv:0911.0091 [hep-ex].
98. K. Hafidi, F.-X. Girod, E. Voutier, H. Egiyan and S. Liuti, JLab Experiment E-08-024 (2006).
99. H. Gao, J. P. Chen, X. Jiang, J. C. Peng and X. Qian, JLab Experiment PR-12-09-14 (2009).
100. S. J. Brodsky, D. S. Hwang and I. Schmidt, *Phys. Lett. B* **530** (2002) 99, arXiv:hep-ph/0201296 [hep-ph].
101. M. Burkardt, *Phys. Rev. D* **88** (2013) 014014, arXiv:1205.2916 [hep-ph].
102. D. Boer *et al.*, arXiv:1108.1713 [nucl-th].
103. A. Accardi *et al.*, *Eur. Phys. J. A* **52** (2016) 268.
104. E. C. Aschenauer *et al.*, arXiv:1409.1633 [physics.acc-ph].
105. S. Abeyratne *et al.*, arXiv:1209.0757 [physics.acc-ph].
106. S. Abeyratne *et al.*, arXiv:1504.07961 [physics.acc-ph].
107. C. Weiss *et al.*, Jefferson Lab 2014/15 Laboratory–directed R&D Project, Available at. https://www.jlab.org/theory/tag/.
108. V. Guzey, D. Higinbotham, C. Hyde, P. Nadel-Turonski, K. Park, M. Sargsian, M. Strikman and C. Weiss, *PoS* **DIS2014** (2014) 234, arXiv:1407.3236 [hep-ph].
109. W. Cosyn, V. Guzey, D. W. Higinbotham, C. Hyde, S. Kuhn, P. Nadel-Turonski, K. Park, M. Sargsian, M. Strikman and C. Weiss, *J. Phys. Conf. Ser.* **543** (2014) 012007.
110. M. Strikman and C. Weiss, arXiv:1706.02244 [hep-ph].